Homogenization approach and Bloch-Floquet theory for band-gap prediction in 2D locally resonant metamaterials

Claudia Comi, Jean-Jacques Marigo

Homogenization approach and Bloch-Floquet theory for band-gap prediction in 2D locally resonant metamaterials

Claudia Comi · Jean-Jacques Marigo

January 25, 2019

Abstract This paper provides a detailed comparison of the two-scale homogenization method and of the Bloch-Floquet theory for the determination of band gaps in locally resonant metamaterials. A medium composed by a stiff matrix with soft inclusions with 2D periodicity is considered and the equivalent mass density of the homogenized medium is explicitly obtained both for in-plane and out-of-plane wave propagation through two-scale asymptotic expansion. The intervals of frequency where the effective mass is negative identify the band gaps of the material. The Bloch-Floquet problem is then considered and, through an asymptotic analysis, its is shown that it leads to the same prediction of the band gaps. The results are confirmed by some examples and the limits of the asymptotic approach are explicitly given and numerically verified.

1 Introduction

Locally resonant metamaterials (LRM) are periodic or quasi-periodic media constituted by different materials, which can exhibit a peculiar dynamic behavior with spectral gaps at frequencies well below those characteristic of Braggs diffraction phenomena. The existence of band-gaps, i.e. frequency ranges where the propagation of real elastic waves is forbidden, is due to the presence of local resonances and has recently attracted a lot of interest in view of a number of potential applications, e.g. for the innovative design of vibration insulators [12], [23], of seismic shields [8], of impact absorbers [9] and of energy harvesters [17]. Various examples of LRM have been reported in the literature, they can be constituted by a periodic structure, made of a single material, with local resonators within the unit cell [12], by three components (e.g. hard inclusions with a soft coating embedded in a hard matrix [16,15] or cellular materials filled by a foam with hard inclusions [10]) or by two materials, typically soft inclusions in hard matrix, as studied e.g. in [22,14]. In this latter case of binary composition, which is also considered in the present work, the metamaterials are also referred to as high-contrast composite materials [5].

The study of wave propagation in LRM, aimed to determine the dispersive properties and the presence of band-gaps, can be tackled in different ways. The two-scale homogenization approach was first proposed in [5] for high-contrast binary elastic composite materials in the long wavelength regime, and then developed in different directions. The extension of the the approach to three-component composite materials was proposed in [6], while in [18,19] the approach for a row of locally resonant inclusions was developed.

C. Comi
Department of Civil and Environmental Engineering, Politecnico di Milano, Piazza Leonardo da Vinci 32, 20133 Milan, Italy E-mail: claudia.comi@polimi.it

J.-J. Marigo
Laboratoire de Mécanique des Solides, École polytechnique, Route de Saclay, 91128 Palaiseau, France E-mail: e-mail: jean-jacques.marigo@polytechnique.edu

In all the above referenced works, the equivalent homogenized medium is characterized by an equivalent mass density that depends on the frequency and that can become negative in the vicinity of the resonant frequencies of the inclusions, thus identifying the stop bands. To overcome the classical hypothesis of wavelength much greater then the characteristic lattice length, the high-frequency asymptotic procedure for homogenization was proposed in [11] and then used in [4] to analyze wave propagation through elastic media that contain periodic arrangements of traction free, or clamped, inclusions.

A different approach, widely employed in various contexts, considers the wave propagation in an infinite periodic media and uses the Bloch-Floquet principles to calculate the dispersion surfaces and to determine the pass and stop bands [7]. In this framework, a popular strategy is the direct numerical simulation, using finite elements, of a unit cell of the periodic material with Bloch-Floquet boundary conditions [1], [20].

The main advantage of homogenization methods with respect to direct numerical solutions of the Bloch-Floquet problem is that they can lead to analytical predictions of the stop and pass bands and thus are more suitable in the design of the metamaterial itself. They allow to obtain *a priori* information on the dependence of the band gaps on the mechanical parameters of the constituents and on the geometry and thus open the way to optimization of the metamaterial for specific applications. On the other hand, homogenization methods are restricted by several hypothesis and the actual range of application is not fully defined.

To the author knowledge, there are very few studies devoted to the comparison of the two approaches. A significant exception is the work of Allaire and coworkers [3] which, however, is focused on the discussion of the equivalent forth order stiffness tensor and not on the band gap prediction.

The aim of the present paper is to establish the link between the two-scale homogenization method and of the Bloch-Floquet theory for the determination of band gaps in 2D LRM. To this purpose in Section 3 we revise the homogenization approach for in-plane and out-of-plane wave propagation in a binary periodic material with circular soft inclusions in a stiff matrix and we obtain the effective mass density in closed form: the intervals of frequency for which the effective mass density becomes negative identify the band gaps. In Section 4, the Bloch-Floquet problem is considered and its properties are presented. The asymptotic analysis of that problem, for given wave number, provides an estimate of the band gaps which turns out to coincide with that obtained through homogenization. The results obtained are illustrated in Section 5 by some examples. The dispersion plots are numerically computed by finite element analysis on a single cell, imposing the Bloch-Floquet boundary conditions with wave vectors belonging to the boundary of the first Brillouin zone and the band gaps thus obtained are compared with the intervals defined with the homogenization approach. The limit of validity of these latter is also set and verified in the numerical examples.

2 Framework

We consider the wave propagation problem in a two-constituents elastic material with 2D periodicity. The main assumptions are the following ones:

1. The body Ω is heterogeneous, made of two materials: the matrix m and the cylindrical inclusions (also referred to as fibers, f) periodically distributed in the plane $x_1 - x_2$, see Figure 1a;
2. The two dimensional Bravais lattice of the material, shown in Figure 1b is characterized by the primitive vectors $\mathbf{a}_1$ and $\mathbf{a}_2$ (which can be non-orthogonal and have different moduli). The unit cell Y^ϵ of the lattice is defined as (see Figure 1c):

$$Y^\epsilon = \{\mathbf{x} \in \mathbb{R}^2 \ : \ \mathbf{x} = \sum_{i=1}^{2} \alpha_i \mathbf{a}_i, \quad -1/2 \leq \alpha_i < 1/2 \quad \forall i \in \{1, 2\}\};$$

3. The reciprocal lattice is also 2D, its two basis vectors are denoted by $\mathbf{A}_i, i = 1, 2$ and defined from the $\mathbf{a}_i$'s by the relations

$$\mathbf{A}_i \cdot \mathbf{a}_j = 2\pi \delta_{ij}, \quad \text{for} \quad i, j = 1, 2$$

where δ_{ij} denotes the Kronecker symbol. The Wigner-Seitz cell of the reciprocal lattice defines the First Brillouin Zone, as shown in Figure 1d.

4. The size $a = \|\mathbf{a}_1 \wedge \mathbf{a}_2\|$ of the unit cell Y^ϵ is small with respect to the considered wavelengths in the matrix material $L_m : a = \epsilon L_m$ with ϵ a dimensionless small parameter;

5. The fiber Y_f^ϵ is constituted by a linear elastic isotropic material with low stiffness. The Lamé's constants of this material are $\epsilon^2 \lambda_f$ and $\epsilon^2 \mu_f$, its volume mass density is ρ_f. The radius of the inclusion is $R^\epsilon = \epsilon R$;

6. The remaining part Y_m^ϵ of the cell is made of a stiff isotropic material with elastic moduli λ_m, μ_m and mass density ρ_m;

7. The characteristic length of the body in the out of plane direction x_3 is very large with respect to the size a.
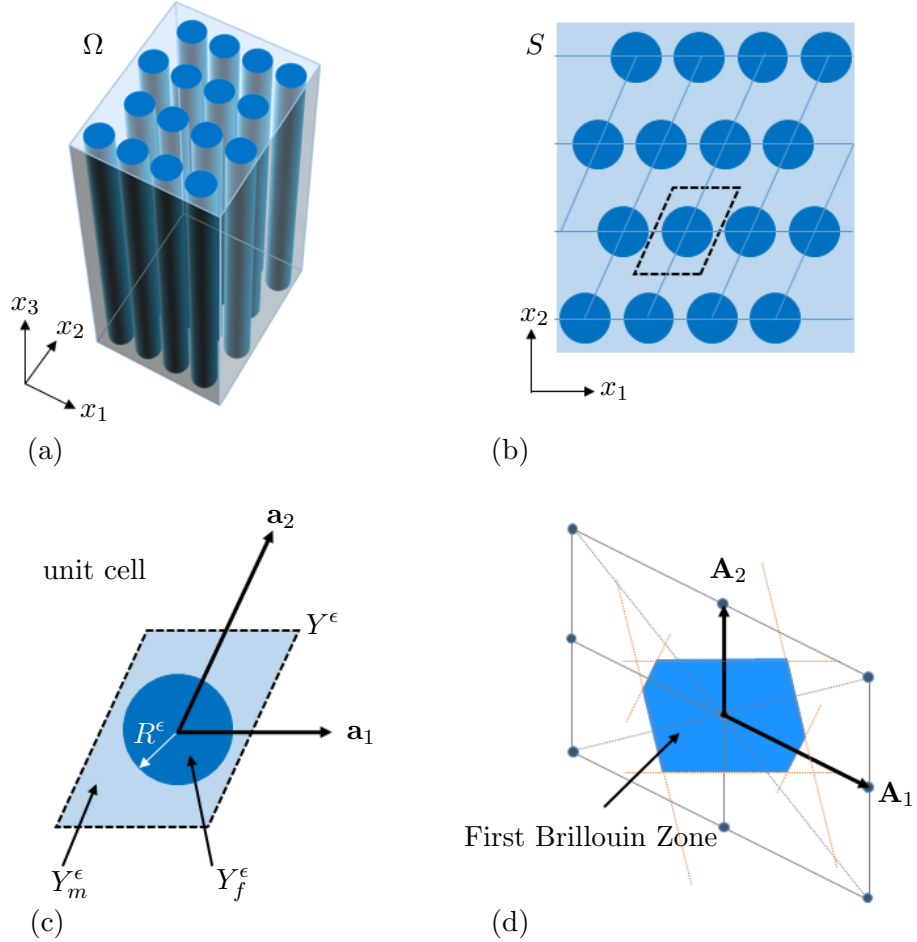
Fig. 1 The 2D periodic material: (a) geometry, (b) 2D lattice, (c) unit cell with basis vectors $\mathbf{a}_i$, (d) reciprocal lattice with basis vectors $\mathbf{A}_i$ and the First Brillouin Zone

The last assumption allows to treat the body as unbounded in the x_3 direction and hence to decouple the problem of wave propagation into two separate problems, one for longitudinal and shear in-plane propagation, and the other for shear waves with out-of-plane polarization. This decoupling is valid for both the homogenization and the Bloch-Floquet approaches, hence in the following we will discuss first the in-plane problem and then we will give the results for the out-of-plane problem.

Notation. Vectors and tensors are represented by bold face letters. An upper index $^{\mathrm{T}}$ denotes transposed quantities. Summation over repeated indices is never implicitly assumed. The complex numbers (or complex fields) are denoted with sans serif letters, like i for $\sqrt{-1}$; the complex conjugate of a complex number is indicated by a superposed bar; the modulus of the complex number u is denoted by $|\mathsf{u}|$. The angular frequency ω is often called just frequency in the text for the sake of brevity.

3 Homogenization approach

3.1 In-plane wave propagation

3.1.1 Main assumptions

We consider a plane motion at given angular frequency ω. Specifically, the displacement field has a vanishing component in the direction 3 and components in the other two directions depending only on (x_1, x_2) (plane strain assumption). That motion is governed by the Helmholtz equation

$$\operatorname{div}\boldsymbol{\sigma}^\epsilon + \rho^\epsilon \omega^2 \mathbf{u}^\epsilon = \mathbf{0} \qquad \text{in} \qquad \Omega \tag{1}$$

where the stress field $\boldsymbol{\sigma}^\epsilon$ is related to the small strain deformation field by the elastic constitutive relation

$$\boldsymbol{\sigma}^\epsilon = \mathbf{E}^\epsilon \boldsymbol{\varepsilon}^\epsilon \qquad \text{in} \qquad \Omega \tag{2}$$

with

$$\boldsymbol{\varepsilon}^\epsilon = \frac{1}{2}(\operatorname{grad} \mathbf{u}^\epsilon + \operatorname{grad}^{\mathrm{T}} \mathbf{u}^\epsilon) \qquad \text{in} \qquad \Omega \tag{3}$$

In (1)-(2), $\mathbf{E}^\epsilon$ and ρ^ϵ denote the (periodic) repartition of the elastic stiffness tensor and the density in the body. In view of the isotropy of the two constituents materials, $\mathbf{E}^\epsilon$ only depends on their Lamé's constants λ and μ and (2) in index notation ($i,j = 1,2$) reads

$$\sigma_{ij}^\epsilon = \lambda^\epsilon (\varepsilon_{11}^\epsilon + \varepsilon_{22}^\epsilon)\delta_{ij} + 2\mu^\epsilon \varepsilon_{ij}^\epsilon \qquad \text{in} \qquad \Omega. \tag{4}$$

Specifically, one has

$$\lambda^\epsilon = \begin{cases} \lambda_m & \text{in} \quad Y_m^\epsilon \\ \epsilon^2 \lambda_f & \text{in} \quad Y_f^\epsilon \end{cases}, \qquad \mu^\epsilon = \begin{cases} \mu_m & \text{in} \quad Y_m^\epsilon \\ \epsilon^2 \mu_f & \text{in} \quad Y_f^\epsilon \end{cases}, \qquad \rho^\epsilon = \begin{cases} \rho_m & \text{in} \quad Y_m^\epsilon \\ \rho_f & \text{in} \quad Y_f^\epsilon \end{cases} \tag{5}$$

In such a plane strain context, the other components of the stress field are given by

$$\sigma_{13}^\epsilon = \sigma_{23}^\epsilon = 0, \qquad \sigma_{33}^\epsilon = \lambda^\epsilon (\varepsilon_{11}^\epsilon + \varepsilon_{22}^\epsilon).$$

Therefore, throughout the present section, all the indices will range in $\{1,2\}$ and all the vectors and tensors will be considered as two-dimensional. The cross-section of the three dimensional domain Ω is denoted by S.

3.1.2 Asymptotic expansions and some properties of the first order terms

The hypotheses listed above allows to use the two-scale asymptotic method [2,21] to construct the homogenized (or effective) equation of motion of the body. Denoting by $\mathbf{x} = (x_1, x_2)$ the (in-plane) macroscopic coordinate, let us introduce the microscopic one $\mathbf{y} = \mathbf{x}/\epsilon$ which lives in the rescaled cell $Y = Y^\epsilon/\epsilon$. The classical two-scale asymptotic method consists in expanding the field $\mathbf{u}^\epsilon$ in the following form:

$$\mathbf{u}^\epsilon(\mathbf{x}) = \mathbf{u}^0(\mathbf{x}, \mathbf{x}/\epsilon) + \epsilon \mathbf{u}^1(\mathbf{x}, \mathbf{x}/\epsilon) + \epsilon^2 \mathbf{u}^2(\mathbf{x}, \mathbf{x}/\epsilon) + \cdots \tag{6}$$

where the fields $\mathbf{u}^i = \mathbf{u}^i(\mathbf{x}, \mathbf{y})$ are defined on $S \times \mathbb{R}^2$ and are Y-periodic with respect to $\mathbf{y}$. In the same manner, the stress field $\boldsymbol{\sigma}^\epsilon$ is expanded in

$$\boldsymbol{\sigma}^\epsilon(\mathbf{x}) = \boldsymbol{\sigma}^0(\mathbf{x}, \mathbf{x}/\epsilon) + \epsilon\boldsymbol{\sigma}^1(\mathbf{x}, \mathbf{x}/\epsilon) + \epsilon^2\boldsymbol{\sigma}^2(\mathbf{x}, \mathbf{x}/\epsilon) + \cdots \tag{7}$$

where the fields $\boldsymbol{\sigma}^i = \boldsymbol{\sigma}^i(\mathbf{x}, \mathbf{y})$ are defined on $S \times \mathbb{R}^2$ and Y-periodic with respect to $\mathbf{y}$. Note that one assumes in (7) that the stress expansion starts at order 0 while it should start *a priori* at order -1 by virtue of (2), (3) and (6). In fact, it is possible to prove that $\boldsymbol{\sigma}^{-1}$ vanishes and assuming that property allows us to simplify the presentation.

Since the terms of the expansions depend on the microscopic and macroscopic coordinates, we must distinguish the partial derivatives with respect to $\mathbf{x}$ or $\mathbf{y}$. Specifically, for a vector function $\mathbf{u}$ of $(\mathbf{x}, \mathbf{y})$, one denotes by $\mathrm{grad}_{\mathbf{x}}\mathbf{u}$ and $\boldsymbol{\varepsilon}_{\mathbf{x}}(\mathbf{u})$ the gradient of $\mathbf{u}$ and its symmetric part with respect to $\mathbf{x}$, and by $\mathrm{grad}_{\mathbf{y}}\mathbf{u}$ and $\boldsymbol{\varepsilon}_{\mathbf{y}}(\mathbf{u})$ the gradient of $\mathbf{u}$ and its symmetric part with respect to $\mathbf{y}$. In the same manner, for a tensor function $\boldsymbol{\sigma}$ of $(\mathbf{x}, \mathbf{y})$, one denotes by $\mathrm{div}_{\mathbf{x}}\boldsymbol{\sigma}$ and $\mathrm{div}_{\mathbf{y}}\boldsymbol{\sigma}$ the divergence of $\boldsymbol{\sigma}$ with respect to $\mathbf{x}$ and $\mathbf{y}$, respectively. In the case where the function depends on one variable only and when there exists no risk of confusion, the gradient and the divergence are denoted classically, without the index.

In the rescaled cell Y, one denotes by Y_m the part occupied by the hard material and by Y_f the part occupied by the soft material of radius $R = R^\epsilon/\epsilon$, see Figure 2.
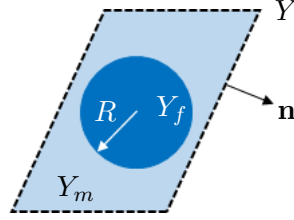
Fig. 2 The rescaled cell of the periodic material with a compliant circular inclusion inside a stiff matrix

From the expansion (6), one gets

$$\boldsymbol{\varepsilon}(\mathbf{u}^\epsilon) = \epsilon^{-1}\boldsymbol{\varepsilon}_{\mathbf{y}}(\mathbf{u}^0) + \left(\boldsymbol{\varepsilon}_{\mathbf{y}}(\mathbf{u}^1) + \boldsymbol{\varepsilon}_{\mathbf{x}}(\mathbf{u}^0)\right) + \epsilon\left(\boldsymbol{\varepsilon}_{\mathbf{y}}(\mathbf{u}^2) + \boldsymbol{\varepsilon}_{\mathbf{x}}(\mathbf{u}^1)\right) + \cdots \tag{8}$$

and from the expansion (7), one gets

$$\mathrm{div}\boldsymbol{\sigma}^\epsilon = \epsilon^{-1}\mathrm{div}_{\mathbf{y}}\boldsymbol{\sigma}^0 + (\mathrm{div}_{\mathbf{y}}\boldsymbol{\sigma}^1 + \mathrm{div}_{\mathbf{x}}\boldsymbol{\sigma}^0) + \epsilon(\mathrm{div}_{\mathbf{y}}\boldsymbol{\sigma}^2 + \mathrm{div}_{\mathbf{x}}\boldsymbol{\sigma}^1) + \cdots \tag{9}$$

The above expansions of the displacement, (6), of the stress, (7), and of their derivatives, (8) and (9), are substituted into the governing equations (1)–(3), then the terms of the same order in ϵ are considered separately.

Inserting (7) and (8) into (2)-(3) gives at order -1

$$\boldsymbol{\varepsilon}_{\mathbf{y}}(\mathbf{u}^0) = \mathbf{0} \quad \text{in} \quad Y_m$$

which, combined with the periodicity conditions, implies that $\mathbf{u}^0$ depends only on $\mathbf{x}$ in $S \times Y_m$, say

$$\mathbf{u}^0(\mathbf{x}, \mathbf{y}) = \mathbf{U}^0(\mathbf{x}) \quad \text{in} \quad S \times Y_m. \tag{10}$$

Equation (1) gives, at order -1 in ϵ:

$$\mathrm{div}_{\mathbf{y}}\boldsymbol{\sigma}^0 = \mathbf{0} \quad \text{in} \quad S \times Y$$

whereas the expansion of (2)-(3) gives at order 0

$$\boldsymbol{\sigma}^0 = \begin{cases} \mathbf{E}_m\left(\boldsymbol{\varepsilon}_{\mathbf{x}}(\mathbf{U}^0) + \boldsymbol{\varepsilon}_{\mathbf{y}}(\mathbf{u}^1)\right) & \text{in} \quad S \times Y_m \\ \mathbf{0} & \text{in} \quad S \times Y_f \end{cases} \tag{11}$$

where $\mathbf{E}_m$ is the isotropic elastic stiffness tensor of the matrix. The term $\boldsymbol{\varepsilon}^0 \equiv \boldsymbol{\varepsilon}_{\mathbf{x}}(\mathbf{U}^0)$ can be interpreted as a constant eigenstrain within the cell of independent components ε_{ij}^0 (namely ε_{11}^0, ε_{22}^0 and $\varepsilon_{12}^0 = \varepsilon_{21}^0$ in the plain strain conditions here considered). By virtue of (10) and using the periodic conditions that $\mathbf{u}^1$ and $\boldsymbol{\sigma}^0\mathbf{n}$ must satisfy on the boundary of Y ($\mathbf{n}$ denoting the unit outer normal), by linearity, one deduces that $\mathbf{u}^1$ can be written in Y_m as

$$\mathbf{u}^1(\mathbf{x},\mathbf{y}) = \sum_{i,j=1}^{2} \varepsilon_{ij}^0(\mathbf{x})\boldsymbol{\chi}^{ij}(\mathbf{y}) + \mathbf{U}^1(\mathbf{x}) \quad \text{in} \quad S \times Y_m, \tag{12}$$

where $\boldsymbol{\chi}^{ij}$, for $i,j = 1,2$, are the displacement fields solutions of the so-called elementary cell problems:

$$\begin{cases} \text{div}_{\mathbf{y}}(\mathbf{E}_m\boldsymbol{\varepsilon}_{\mathbf{y}}(\boldsymbol{\chi}^{ij})) = \mathbf{0} & \text{in} \quad Y_m \\ \mathbf{E}_m(\boldsymbol{\varepsilon}_{\mathbf{y}}(\boldsymbol{\chi}^{ij}) + \mathbf{e}_i \odot \mathbf{e}_j)\,\mathbf{n} = \mathbf{0} & \text{on} \quad \partial Y_f \\ \boldsymbol{\chi}^{ij} \quad \text{periodic}, (\mathbf{E}_m\boldsymbol{\varepsilon}_{\mathbf{y}}(\boldsymbol{\chi}^{ij}))\mathbf{n} \quad \text{anti-periodic} & \text{on} \quad \partial Y \end{cases} \tag{13}$$

where $\mathbf{e}_i$ is the unit vector in the direction i and $\odot$ denotes the symmetric tensorial product ($2\mathbf{e}_i \odot \mathbf{e}_j = \mathbf{e}_i \otimes \mathbf{e}_j + \mathbf{e}_j \otimes \mathbf{e}_i$). The solution of each elementary cell problem is defined up to a constant which can be fixed by imposing that

$$\int_{Y_m} \boldsymbol{\chi}^{ij}(\mathbf{y})d\mathbf{y} = \mathbf{0}.$$

The elementary cell problems are classical in homogenization theory, note however that here problems (13) correspond to the case where the soft material is replaced by a cavity.

By virtue of (11) and (10), the stress field $\boldsymbol{\sigma}^0$ can read as

$$\boldsymbol{\sigma}^0(\mathbf{x},\mathbf{y}) = \begin{cases} \sum_{i,j=1}^{2} \mathbf{E}_m(\boldsymbol{\varepsilon}_{\mathbf{y}}(\boldsymbol{\chi}^{ij})(\mathbf{y}) + \mathbf{e}_i \odot \mathbf{e}_j)\varepsilon_{ij}^0(\mathbf{x}) & \text{in} \quad S \times Y_m \\ \mathbf{0} & \text{in} \quad S \times Y_f \end{cases}. \tag{14}$$

Taking the average value of $\boldsymbol{\sigma}^0$ on Y and using (13) one obtains

$$\langle\boldsymbol{\sigma}^0\rangle(\mathbf{x}) := \frac{1}{|Y|}\int_Y \boldsymbol{\sigma}^0(\mathbf{x},\mathbf{y})d\mathbf{y} = \mathbf{E}^*\boldsymbol{\varepsilon}^0(\mathbf{x}) \tag{15}$$

where $\mathbf{E}^*$ denotes the fourth order tensor whose components are given by

$$E_{ijkl}^* = \frac{1}{|Y|}\int_{Y_m} \mathbf{E}_m\left(\boldsymbol{\varepsilon}_{\mathbf{y}}(\boldsymbol{\chi}^{ij}) + \mathbf{e}_i \odot \mathbf{e}_j\right) \cdot \left(\boldsymbol{\varepsilon}_{\mathbf{y}}(\boldsymbol{\chi}^{kl}) + \mathbf{e}_k \odot \mathbf{e}_l\right)d\mathbf{y}. \tag{16}$$

In (16) the dot denotes the tensor scalar product: $\mathbf{A} \cdot \mathbf{B} = \sum_{r,s=1}^{2} A_{rs}B_{rs}$. The tensor $\mathbf{E}^*$ represents the in-plane effective stiffness tensor of the matrix with a cavity inside. That tensor is symmetric and definite positive. It corresponds to the stiffness of an elastic anisotropic material, which can be isotropic (in the plane) if the cell is sufficiently symmetric.

3.1.3 In-plane eigenvibrations of the inclusion fixed at its boundary

Before to continue the asymptotic analysis of the equation of motion, let us characterize the in-plane eigenmodes of vibration and the associated eigenfrequencies of an inclusion with Dirichlet boundary conditions. The eigenmode $\boldsymbol{\eta}_* \neq \mathbf{0}$ and the associated eigenfrequency ω_* are solution of

$$\begin{cases} (\lambda_f + \mu_f)\text{grad}_{\mathbf{y}}\text{div}_{\mathbf{y}}\boldsymbol{\eta}_* + \mu_f\Delta_{\mathbf{y}}\boldsymbol{\eta}_* + \rho_f\omega_*^2\boldsymbol{\eta}_* = \mathbf{0} & \text{in} \quad Y_f \\ \boldsymbol{\eta}_* = \mathbf{0} & \text{on} \quad \partial Y_f \end{cases}, \tag{17}$$

6

where $\Delta_{\mathbf{y}} \equiv \frac{\partial^2}{\partial y_1^2} + \frac{\partial^2}{\partial y_2^2}$ is the two dimensional Laplace operator. From the classical spectral theorem for self-adjoint compact operators, it follows that: (i) there exists a countable family of eigenfrequencies; (ii) the eigenmodes associated to an eigenfrequency constitute a linear space of finite dimension (called the eigenspace); (iii) the family of all the eigenmodes constitutes an orthogonal basis (in the sense of the $L^2(Y_f)$ inner product) of the space of smooth in-plane displacement fields defined in Y_f and vanishing on ∂Y_f.

In the present case of a circular inclusion Y_f, that eigenvalue problem can be solved in closed form. We only give the main results without the details of the calculations. In view of the geometry, polar coordinates r and ϑ are adopted:

$$\mathbf{y} = r\cos\vartheta\,\mathbf{e}_1 + r\sin\vartheta\,\mathbf{e}_2, \quad r \in [0, R], \quad \vartheta \in [0, 2\pi].$$

The eigenmodes can be expressed as

$$\boldsymbol{\eta}_*(\mathbf{y}) = f_*(r)\cos(p\vartheta + \theta_0)\mathbf{e}_r + g_*(r)\sin(p\vartheta + \theta_0)\mathbf{e}_\vartheta \tag{18}$$

with $p \in \mathbb{N}$, θ_0 an arbitrary constant, $\mathbf{e}_r$ and $\mathbf{e}_\vartheta$ the unit vectors in the radial and tangential directions. The two functions of r are given by

$$\begin{cases} f_*(r) &= a_*\Big(J_{p-1}(k_*^s r) + J_{p+1}(k_*^s r)\Big) + b_*\Big(J_{p-1}(k_*^l r) - J_{p+1}(k_*^l r)\Big) \\ g_*(r) &= a_*\Big(J_{p-1}(k_*^s r) - J_{p+1}(k_*^s r)\Big) + b_*\Big(J_{p-1}(k_*^l r) + J_{p+1}(k_*^l r)\Big) \end{cases} \tag{19}$$

where J_p denotes the Bessel function of first kind and order p, a_* and b_* are constants. In (19), k_*^l and k_*^s are the rescaled longitudinal and shear wave numbers for the inclusion, corresponding to the eigenfrequency ω_* and defined as

$$k_*^l = \omega_*\sqrt{\frac{\rho_f}{\lambda_f + 2\mu_f}} = \frac{\omega_*}{c_l}, \qquad k_*^s = \omega_*\sqrt{\frac{\rho_f}{\mu_f}} = \frac{\omega_*}{c_s} \tag{20}$$

where c_l and c_s are the scaled velocities of propagation of longitudinal and shear waves. To fulfill the boundary condition $\boldsymbol{\eta}_* = \mathbf{0}$ on ∂Y_f, the pair $(a_*, b_*) \neq (0, 0)$ must satisfy

$$J_{p-1}(k_*^s R)a_* = -J_{p-1}(k_*^l R)b_*, \qquad J_{p+1}(k_*^s R)a_* = J_{p+1}(k_*^l R)b_*,$$

this is possible if ω_* is a solution of

$$den_p \equiv J_{p-1}(k_*^s R)J_{p+1}(k_*^l R) + J_{p-1}(k_*^l R)J_{p+1}(k_*^s R) = 0. \tag{21}$$

This latter equation gives the eigenfrequencies with mode number p; they constitute a countable family of positive real numbers $\omega_n^p, n \in \mathbb{N}^*$. Moreover, for $p > 0$, the eigenspaces are (at least) of dimension 2. As far as the properties of orthogonality of the eigenmodes with the translations is concerned, one must distinguish the case $p = 1$ from the other ones.

When $p \neq 1$, the eigenmodes are orthogonal to the translations, *i.e.* the following equalities hold true:

$$\int_{Y_f} \boldsymbol{\eta}_*(\mathbf{y}) \cdot \mathbf{e}_1 d\mathbf{y} = \int_{Y_f} \boldsymbol{\eta}_*(\mathbf{y}) \cdot \mathbf{e}_2 d\mathbf{y} = 0. \tag{22}$$

When $p = 1$, then an eigenfrequency ω_* is solution of the following equation:

$$J_0(k_*^s R)J_2(k_*^l R) + J_0(k_*^l R)J_2(k_*^s R) = 0. \tag{23}$$

Accordingly, there exists a sequence denoted $\omega_n, n \in \mathbb{N}^*$ (where the superscript $p = 1$ is omitted to simplify the notation), of eigenfrequencies solutions of (23). Those frequencies ω_n can be expressed as

$$\omega_n = \zeta_n \frac{c_l}{R} \tag{24}$$

with ζ_n real numbers depending on the ratio between the longitudinal and the shear velocities, i.e. on the Poisson's coefficient of the inclusion ν_f

$$\frac{c_l}{c_s} = \sqrt{\frac{2(1-\nu_f)}{1-2\nu_f}} := c(\nu_f).$$ (25)

Table 1 and Figure 3 report the coefficients ζ_n of the first three eigenfrequencies for different Poisson's coefficients.

ν_f	ζ_1	ζ_2	ζ_3
0	2.07516	3.77206	5.31666
0.2	1.97804	3.28481	5.14909
0.4	1.74608	2.2812	3.48963
0.49	0.715047	1.16922	1.59712

Table 1 Coefficients ζ_n of the first three eigenfrequencies of the inclusion associated with the eigenmode number $p = 1$ for several values of ν_f.
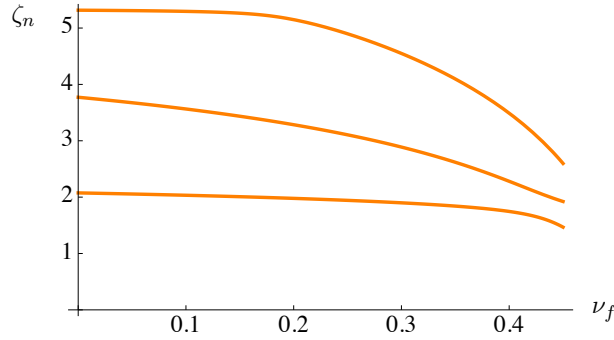
Fig. 3 Coefficients ζ_n of the first three eigenfrequencies of the inclusion associated with the eigenmode number $p = 1$ vs Poisson's ratio ν_f of the inclusion.

The two corresponding eigenmodes are given by:

$$\boldsymbol{\eta}_*^{①}(\mathbf{y}) = f_*(r)\cos\vartheta\mathbf{e}_r - g_*(r)\sin\vartheta\mathbf{e}_\vartheta, \qquad \boldsymbol{\eta}_*^{②}(\mathbf{y}) = f_*(r)\sin\vartheta\mathbf{e}_r + g_*(r)\cos\vartheta\mathbf{e}_\vartheta$$ (26)

where the two functions f_* and g_* read

$$\begin{cases} f_*(r) &= a_*\left(J_0(k_*^s r) + J_2(k_*^s r)\right) + b_*\left(J_0(k_*^l r) - J_2(k_*^l r)\right) \\ g_*(r) &= a_*\left(J_0(k_*^s r) - J_2(k_*^s r)\right) + b_*\left(J_0(k_*^l r) + J_2(k_*^l r)\right) \end{cases}.$$ (27)

The pair $(a_*, b_*) \neq (0,0)$ must satisfy

$$J_0(k_*^s R)a_* = -J_0(k_*^l R)b_*, \qquad J_2(k_*^s R)a_* = J_2(k_*^l R)b_*,$$ (28)

that is possible by virtue of (23). The inner product of the two eigenmodes with the translations $\mathbf{e}_1$ and $\mathbf{e}_2$ reads

$$\int_{Y_s} \boldsymbol{\eta}_*^{①} \cdot \mathbf{e}_1 d\mathbf{y} = \int_{Y_s} \boldsymbol{\eta}_*^{②} \cdot \mathbf{e}_2 d\mathbf{y} = 2\pi R^2 J_2(k_*^s R)a_* = -2\pi R^2 J_2(k_*^l R)b_*$$

$$\int_{Y_s} \boldsymbol{\eta}_*^{①} \cdot \mathbf{e}_2 d\mathbf{y} = \int_{Y_s} \boldsymbol{\eta}_*^{②} \cdot \mathbf{e}_1 d\mathbf{y} = 0.$$

So, the eigenmodes are orthogonal to the translations if and only if $J_2(k_*^l R)J_2(k_*^s R) = 0$, condition which can be written as

$$J_2(\zeta_n)J_2\big(c(\nu_f)\zeta_n\big) = 0 \tag{29}$$

and depends on the Poisson ratio ν_f and the number of the eigenfrequency. In general, the two n^{th} eigenmodes are not orthogonal to the translations, except for particular values of the Poisson ratio. Numerical computations show that for $n = 1$ and $n = 2$, equation (29) has no solution in the range $0 \leq \nu_f < 0.5$ (see Figure 4a for $n = 1$), hence the first ($n = 1$) and the second ($n = 2$) eigenmodes are never orthogonal to the translations. On the contrary, as one can see on Figure 4b, both $J_2(\zeta_3)$ and $J_2(c\zeta_3)$ vanish for the value $\nu_f = \nu_* \approx 0.2035$ and hence the third eigenmodes are orthogonal to the translations for $\nu_f = \nu_*$.
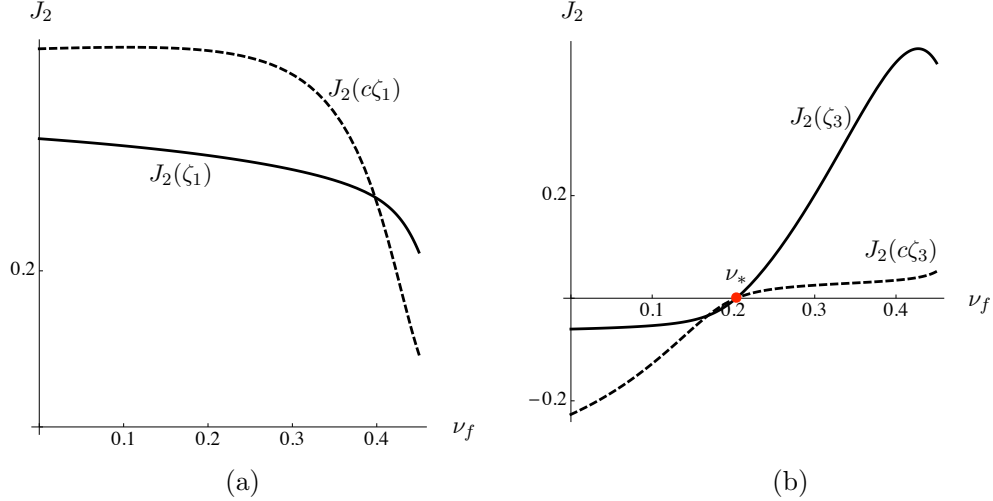
Fig. 4 Graphs of (a) $J_2(\zeta_1)$ and $J_2(c\zeta_1)$ and (b) $J_2(\zeta_3)$ and $J_2(c\zeta_3)$ as functions of the Poisson coefficient ν_f. At $\nu_f = \nu_* \approx 0.2035$ condition (29) if fulfilled with $n = 3$, hence the third eigenmodes are orthogonal to the translations for $\nu_f = \nu_*$.

3.1.4 The motion problem for the soft inclusion

The expansion of the equation of motion (1) gives at order 0 in the inclusion

$$\text{div}_{\mathbf{y}}\boldsymbol{\sigma}^1 + \rho_f\omega^2\mathbf{u}^0 = \mathbf{0} \quad \text{in} \quad S \times Y_f \tag{30}$$

where we have used the fact that $\boldsymbol{\sigma}^0 = \mathbf{0}$ in Y_f. The expansion of the constitutive relation at order 1 in Y_f gives

$$\boldsymbol{\sigma}^1 = \mathbf{E}_f\boldsymbol{\varepsilon}_{\mathbf{y}}(\mathbf{u}^0) \quad \text{in} \quad S \times Y_f, \tag{31}$$

where $\mathbf{E}_f$ is the rescaled stiffness tensor of the inclusion. Inserting (31) into (30) and using the continuity of the displacement at the interface between the soft and the hard material lead to the following local problem governing the motion of the inclusion:

$$\begin{cases} (\lambda_f + \mu_f)\text{grad}_{\mathbf{y}}\text{div}_{\mathbf{y}}\mathbf{u}^0 + \mu_f\Delta_{\mathbf{y}}\mathbf{u}^0 + \rho_f\omega^2\mathbf{u}^0 = \mathbf{0} & \text{in} \quad S \times Y_f \\ \mathbf{u}^0 = \mathbf{U}^0 & \text{on} \quad S \times \partial Y_f \end{cases} \tag{32}$$

For a given ω and a given $\mathbf{U}^0$, problem (32) admits a unique solution $\mathbf{u}^0$ provided that ω is not a frequency of resonance of the clamped inclusion. Specifically, in that case, by linearity, $\mathbf{u}^0$ can read as

$$\mathbf{u}^0(\mathbf{x}, \mathbf{y}) = \sum_{i=1}^{2} U_i^0(\mathbf{x})\boldsymbol{\eta}^{\oplus}(\mathbf{y}) \quad \text{in} \quad S \times Y_f \tag{33}$$

9

where $\boldsymbol{\eta}^{\textcircled{i}}$, for $i = 1$ or 2, must satisfy (at given ω) the following PDE:

$$(\lambda_f + \mu_f)\mathrm{grad}_{\mathbf{y}}\mathrm{div}_{\mathbf{y}}\boldsymbol{\eta}^{\textcircled{i}} + \mu_f\Delta_{\mathbf{y}}\boldsymbol{\eta}^{\textcircled{i}} + \rho_f\omega^2(\mathbf{e}_i + \boldsymbol{\eta}^{\textcircled{i}}) = \mathbf{0} \quad \text{in} \quad Y_f \tag{34}$$

with the boundary conditions

$$\boldsymbol{\eta}^{\textcircled{i}} = \mathbf{0} \quad \text{on} \quad \partial Y_f. \tag{35}$$

Let us first discuss the existence and the uniqueness of the solution of problem (34)-(35) depending on the value of ω. One has the following alternatives:

(i) *If ω is not an eigenfrequency, the solution of (34)-(35) is unique.*

(ii) *If ω is an eigenfrequency whose eigenspace is orthogonal to the translations, the problem (34)-(35) admits a (non unique) solution defined up to an arbitrary eigenmode.*

(iii) *If ω is an eigenfrequency with some eigenmodes non orthogonal to the translations, the problem (34)-(35) does not admit a solution.*

The proofs of those properties are direct consequences of the modal decomposition of (34). This problem can be solved in closed form in the case of a circular inclusion.

In case (i), where ω is not an eigenfrequency, the unique solution is of the form

$$\boldsymbol{\eta}^{\textcircled{1}}(\mathbf{y}) = \eta_r(r)\cos\vartheta\mathbf{e}_r - \eta_\vartheta(r)\sin\vartheta\mathbf{e}_\vartheta, \qquad \boldsymbol{\eta}^{\textcircled{2}}(\mathbf{y}) = \eta_r(r)\sin\vartheta\mathbf{e}_r + \eta_\vartheta(r)\cos\vartheta\mathbf{e}_\vartheta. \tag{36}$$

One deduces from (34) that the two functions of r, η_r and η_ϑ, are given by

$$\begin{cases} \eta_r(r) &= a\Big(J_0(k^s r) + J_2(k^s r)\Big) + b\Big(J_0(k^l r) - J_2(k^l r)\Big) - 1 \\ \eta_\vartheta(r) &= a\Big(J_0(k^s r) - J_2(k^s r)\Big) + b\Big(J_0(k^l r) + J_2(k^l r)\Big) - 1 \end{cases} \tag{37}$$

In (37), k^l and k^s are the rescaled longitudinal and shear wave numbers for the inclusion, corresponding to a given angular frequency ω and defined as

$$k^l = \frac{\omega}{c_l}, \qquad k^s = \frac{\omega}{c_s}. \tag{38}$$

By virtue of (35), the constants a and b must be such that $\eta_r(R) = \eta_\vartheta(R) = 0$. One deduces from that linear system that the constants a and b are given by

$$a = \frac{J_2(k^l R)}{den}, \qquad b = \frac{J_2(k^s R)}{den} \tag{39}$$

provided that the denominator *den* which reads

$$den \equiv J_0(k^s R)J_2(k^l R) + J_0(k^l R)J_2(k^s R) \tag{40}$$

does not vanish. Accordingly, by virtue of (23), a and b are well defined by (39) provided that $\omega \neq \omega_n, n \in \mathbb{N}^*$, ω_n being the eigenfrequencies of the inclusion associated with the eigenmode number $p = 1$.

In the case (ii) one should distinguish two situations: case (iia) the eigenfrequency ω_* does not satisfy (23); case (iib) the eigenfrequency ω_* satisfies (23) and its eigenspace is orthogonal to the translations.

In the case (iia) which corresponds to an eigenmode number $p \neq 1$, the solution of (34)-(35) is defined up to an eigenmode. Accordingly, the solution reads as

$$\begin{cases} \boldsymbol{\eta}^{\textcircled{1}}(\mathbf{y}) = \eta_r(r)\cos\vartheta\mathbf{e}_r - \eta_\vartheta(r)\sin\vartheta\mathbf{e}_\vartheta + \boldsymbol{\eta}^{\textcircled{1}}_*(\mathbf{y}), \\ \boldsymbol{\eta}^{\textcircled{2}}(\mathbf{y}) = \eta_r(r)\sin\vartheta\mathbf{e}_r + \eta_\vartheta(r)\cos\vartheta\mathbf{e}_\vartheta + \boldsymbol{\eta}^{\textcircled{2}}_*(\mathbf{y}) \end{cases} \tag{41}$$

where η_r and η_ϑ are still given by (37)–(40) whereas $\boldsymbol{\eta}^{\textcircled{1}}_*$ and $\boldsymbol{\eta}^{\textcircled{2}}_*$ are two arbitrary eigenmodes.

In the case (iib), the eigenmode number $p = 1$, the solution of (34)-(35) still exists and is defined up to an eigenmode (its general expression is not given here). Such a case holds for instance when $\nu_f = \nu_* \approx 0.2035$ and $\omega = \omega_3$ as discussed in Section 3.1.3. In this particular case where both $J_2(k^s R)$ and $J_2(k^l R)$ vanishes, the solutions $\boldsymbol{\eta}^{\textcircled{1}}$ and $\boldsymbol{\eta}^{\textcircled{2}}$ of (34)-(35) are given by (36)-(37) with a and b related by

$$aJ_0(k^s R) + bJ_0(k^s R) = 1. \tag{42}$$

Finally, when ω is an eigenfrequency which satisfies (23) and whose eigenspace is not orthogonal to the translation (case (iii)), the problem (34)-(35) has no solution.

3.1.5 The effective in-plane motion problem for the composite

One can only consider the cases (i) and (ii) where the problem (34)-(35) admits a solution, because in the case (iii) where the problem (34)-(35) has no solution, from (32) one should have $\mathbf{U}^0 = \mathbf{0}$.

The expansion of the equation of motion gives at the order 0 in the whole cell

$$\text{div}_{\mathbf{y}}\boldsymbol{\sigma}^1 + \text{div}_{\mathbf{x}}\boldsymbol{\sigma}^0 + \rho\omega^2\mathbf{u}^0 = \mathbf{0} \quad \text{in} \quad S \times Y. \tag{43}$$

Integrating this equation over Y leads to the following expressions for the different terms:

$$\int_Y \text{div}_{\mathbf{y}}\boldsymbol{\sigma}^1 d\mathbf{y} = \int_{\partial Y} \boldsymbol{\sigma}^1\mathbf{n}\,dS = \mathbf{0} \quad \text{by virtue of the periodic conditions}$$

$$\langle\text{div}_{\mathbf{x}}\boldsymbol{\sigma}^0\rangle = \text{div}\langle\boldsymbol{\sigma}^0\rangle = \text{div}\Big(\mathbf{E}^*\,\boldsymbol{\varepsilon}(\mathbf{U}^0)\Big) \text{ by virtue of (15)}$$

$$\langle\rho\mathbf{u}^0\rangle = \boldsymbol{\rho}^*(\omega)\mathbf{U}^0 \qquad \text{by virtue of (10) and (33)}$$

where $\boldsymbol{\rho}^*(\omega)$ is a 2×2 matrix whose entries are given by

$$\rho^*_{ij}(\omega) = \rho_{st}\delta_{ij} + \frac{\rho_f}{|Y|}\int_{Y_f} \eta_j^\odot(\mathbf{y})d\mathbf{y}. \tag{44}$$

In (44) ρ_{st} denotes the equivalent static mass density of the material,

$$\rho_{st} = \rho_m\frac{|Y_m|}{|Y|} + \rho_f\frac{|Y_f|}{|Y|}. \tag{45}$$

Finally the effective equation of motion reads

$$\text{div}\Big(\mathbf{E}^*\boldsymbol{\varepsilon}(\mathbf{U}^0)\Big) + \boldsymbol{\rho}^*(\omega)\omega^2\mathbf{U}^0 = \mathbf{0} \quad \text{in} \quad S. \tag{46}$$

Thus, $\boldsymbol{\rho}^*(\omega)$ can be interpreted as the matrix of the (in-plane) effective mass density of the composite material. It depends on the frequency because of the dependence of $\boldsymbol{\eta}^\odot$ on ω. Let us first note that $\boldsymbol{\rho}^*(\omega)$ is well defined even when the solution $\boldsymbol{\eta}^\odot$ of (34)-(35) is not unique. Indeed, that corresponds to the case (ii) where ω is an eigenfrequency whose eigenspace is orthogonal to the translations and then $\boldsymbol{\eta}^\odot$ is defined up to an eigenmode $\boldsymbol{\eta}_*$. Therefore, since $\int_{Y_f} \boldsymbol{\eta}_* \cdot \mathbf{e}_1 d\mathbf{y} = \int_{Y_f} \boldsymbol{\eta}_* \cdot \mathbf{e}_2 d\mathbf{y} = 0$, $\int_{Y_f} \eta_j^\odot d\mathbf{y}$ is determined. Let us also note that $\boldsymbol{\rho}^*(\omega)$ does not depend on the stiffness of the hard material, but only on the volume fraction and the mass density of the materials, and on the geometry and the stiffness of the soft inclusion.

In the case of a circular inclusion, $\boldsymbol{\rho}^*(\omega)$ is obtained in closed form. Let us first consider the cases (i) and (iia) of the previous subsection 3.1.4. Using (36) one easily checks that $\int_{Y_f} \eta_j^\odot(\mathbf{y})d\mathbf{y} = 0$ for $i \neq j$ and that $\rho^*_{11} = \rho^*_{22}$. Therefore $\boldsymbol{\rho}^*(\omega)$ can read as

$$\boldsymbol{\rho}^*(\omega) = \rho^*(\omega)\mathbf{I}.$$

Using (37)–(40) one obtains

$$\rho^*(\omega) = \rho_{st} + \rho_f\frac{|Y_f|}{|Y|}\frac{2J_2(k^lR)J_2(k^sR)}{J_0(k^sR)J_2(k^lR) + J_0(k^lR)J_2(k^sR)} \qquad \text{for} \quad \omega \neq 0. \tag{47}$$

When $\omega = 0$, one finds directly from (34)-(35) that $\boldsymbol{\eta}^\odot = \mathbf{0}$ in Y_f and hence $\rho^*(0) = \rho_{st}$.

Figure 5 shows the variation of the effective mass density (normalized with the static one) with the normalized frequency ω/ω_1. Note that this normalized plot only depends on ν_f, which is fixed to 0.4 in Figure 5. Thus, $\rho^*(\omega)$ is not defined when $\omega = \omega_n = \zeta_n c_l/R$ with $n \in \mathbb{N}^*$, tends to $-\infty$ and $+\infty$ when ω tends to ω_n from above and from below, respectively, and it is strictly increasing in every interval (ω_n, ω_{n+1}). Consequently, the effective mass density is not positive in a countable family of intervals I_n of the form

$$I_n = \left[\zeta_n\frac{c_l}{R}, \theta_n\right], \quad n \in \mathbb{N}^*, \tag{48}$$
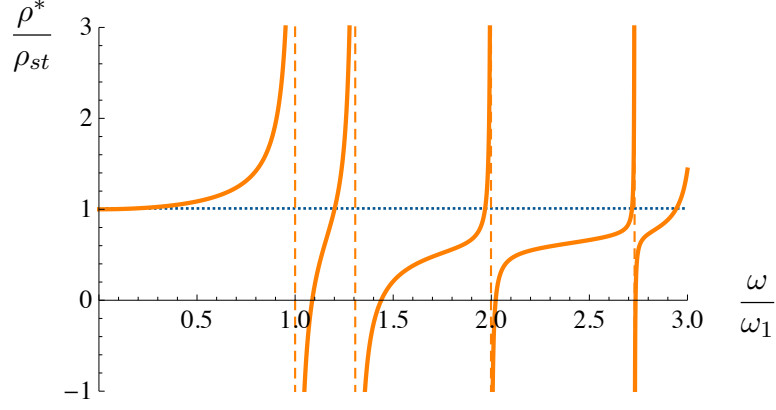
Fig. 5 Normalized effective mass vs. normalized frequency for $\nu_f = 0.4$. The intervals of negative effective mass give the first four band gaps. The mass ratio between matrix and inclusion is 1.41 and it corresponds to the material considered in Section 5.

where θ_n are the frequencies corresponding to $\rho^* = 0$.

In the particular case (iib) of the previous subsection 3.1.4 when $\nu_f = \nu_* \approx 0.2035$ and $\omega = \omega_3$, using (36), (37) and (42) one has $\int_{Y_f} \eta_j^i d\mathbf{y} = 0$ and hence $\rho^*(\omega_3) = \rho_{st}$. Figure 6 compares the variation of the effective mass density in the cases $\nu_f = \nu_* = 0.2035$ (left) and ν_f close (but not equal) to ν_* (right). When $\nu = \nu_*$, even though $\omega_3 \approx 2.6\omega_1$ is an eigenfrequency, since its eigenspace is orthogonal to the translations, $\rho^*(\omega_3)$ is well defined (and equal to ρ_{st}) and there is no interval near ω_3 where ρ^* is negative. Therefore, as it will be discussed in the next subsection, no band gap exists opening at ω_3. If one considers ν_f slightly different from ν_* (equal to 0.23 in Figure 6 on the right), since the eigenspace associated with ω_3 is no more orthogonal to the translations, then $\rho^*(\omega_3)$ is no more defined and it exists an interval on the right of ω_3 where ρ^* is negative. Accordingly, there is a band gap opening at ω_3. However the width of the band gap is small (within the line thickness in Figure 6, right). In fact the closer ν to ν_* and the smaller the width of the band gap near ω_3; at the limit, when $\nu = \nu_*$ the band gap disappears.
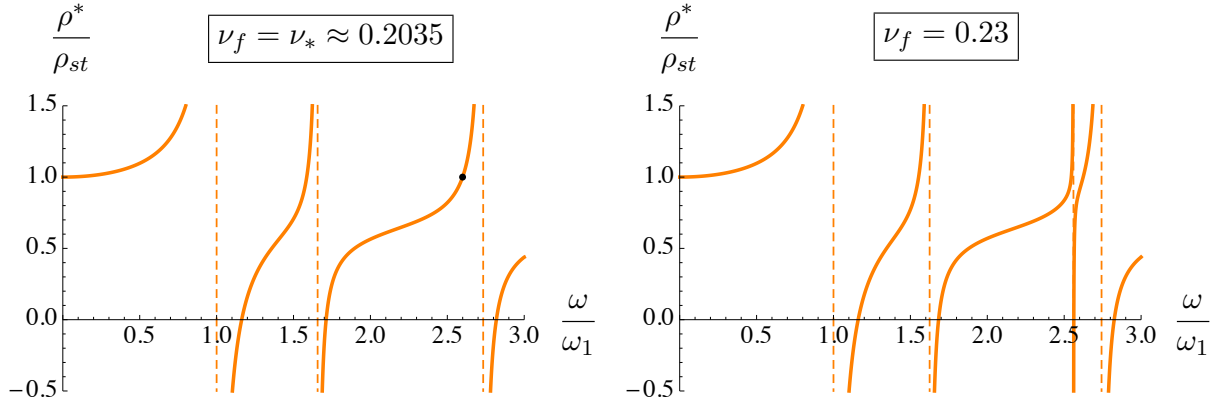
Fig. 6 Normalized effective mass vs. normalized frequency for $\nu_f = \nu_*$ (left) and $\nu_f = 0.23$ (right).

3.1.6 The band gaps

Let us consider the effective equation of motion (46) and a solution corresponding to an harmonic wave of the form

$$\mathbf{U}^0(\mathbf{x}, t) = \exp \mathrm{i}(k\mathbf{m} \cdot \mathbf{x} - \omega t)\boldsymbol{\xi},$$

12

where ω and $\mathbf{m}$ denote the given angular frequency and direction of propagation whereas $\boldsymbol{\xi}$ and k are the non zero polarization vector and wave number to be determined. Such a wave with wave vector $\mathbf{k} = k\mathbf{m}$ can propagate inside the composite material provided that k and $\boldsymbol{\xi}$ satisfy the following problem:

$$\mathbf{Q}^*(\mathbf{m})\boldsymbol{\xi} = \rho^*(\omega)\frac{\omega^2}{k^2}\boldsymbol{\xi}, \tag{49}$$

where $\mathbf{Q}^*(\mathbf{m})$ denotes the effective acoustic tensor associated with the direction of propagation $\mathbf{m}$:

$$Q_{ih}^*(\mathbf{m}) = \sum_{j,l=1}^{2} E_{ijhl}^* m_j m_l. \tag{50}$$

Since $\mathbf{Q}^*(\mathbf{m})$ is positive definite, the wave number k is a real positive number if and only if the effective mass density $\rho^*(\omega)$ is positive. Therefore, by virtue of the previous analysis, harmonic waves can only propagate if the frequency ω lies outside the intervals I_n, $n \in \mathbb{N}^*$, defined by (48) which thus identify the band gaps.

Let us return to the real physical quantities instead of the rescaled ones. The real wave velocities in the inclusion are $c_l^\epsilon = \epsilon c_l$, $c_s^\epsilon = \epsilon c_s$ and the real diameter of the inclusion is $2R^\epsilon = 2\epsilon R$. Therefore $c_l^\epsilon/R^\epsilon = c_l/R$ and the frequencies ω_n previously introduced can be interpreted as characteristic frequencies of the real inclusion. Hence the intervals I_n turn out to depend only on the mass ratio between the hard and the soft material and on the Poisson's coefficient of the inclusion. Figure 7 shows the dependence of the first band gap on ν_f, the relative amplitude increases as ν_f decreases.
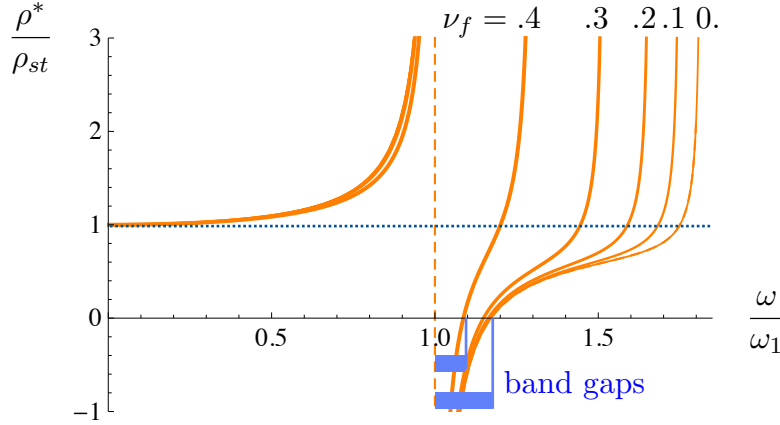
Fig. 7 Normalized effective mass vs. normalized frequency for varying ν_f. The intervals of negative effective mass give the first band gap. The mass ratio between matrix and inclusion is 1.41 and corresponds to the material considered in Section 5.

3.2 Out-of-plane wave propagation

The same procedure followed for in-plane polarized waves can be used for waves with out-of-plane polarization.

3.2.1 Asymptotic expansions and some properties of the first order terms

Specifically, one assumes now that the displacement field has only a component in the third direction and that it depends only on (x_1, x_2) (anti-plane strain condition):

$$\mathbf{u}^\epsilon(\mathbf{x}) = u^\epsilon(x_1, x_2)\mathbf{e}_3.$$

Therefore the non vanishing stress components are $\sigma_{31}^\epsilon = \sigma_{13}^\epsilon$ and $\sigma_{32}^\epsilon = \sigma_{23}^\epsilon$. Hence we will consider that the stress field is the vector field $\boldsymbol{\sigma}^\epsilon(x_1, x_2) = \left(\sigma_{31}^\epsilon(x_1, x_2), \sigma_{32}^\epsilon(x_1, x_2)\right)$ which is defined on S and related to u^ϵ by

$$\boldsymbol{\sigma}^\epsilon = \mu^\epsilon \operatorname{grad} u^\epsilon \qquad \text{in} \qquad S. \tag{51}$$

The equation of motion (1) in this case becomes

$$\operatorname{div}\boldsymbol{\sigma}^\epsilon + \rho^\epsilon \omega^2 u^\epsilon = 0 \qquad \text{in} \qquad S. \tag{52}$$

The expansions of u^ϵ and $\boldsymbol{\sigma}^\epsilon$ with respect to ϵ read

$$u^\epsilon(\mathbf{x}) = u^0(\mathbf{x}, \mathbf{x}/\epsilon) + \epsilon u^1(\mathbf{x}, \mathbf{x}/\epsilon) + \epsilon^2 u^2(\mathbf{x}, \mathbf{x}/\epsilon) + \cdots \tag{53}$$

$$\boldsymbol{\sigma}^\epsilon(\mathbf{x}) = \boldsymbol{\sigma}^0(\mathbf{x}, \mathbf{x}/\epsilon) + \epsilon\boldsymbol{\sigma}^1(\mathbf{x}, \mathbf{x}/\epsilon) + \epsilon^2\boldsymbol{\sigma}^2(\mathbf{x}, \mathbf{x}/\epsilon) + \cdots \tag{54}$$

where the fields $u^i = u^i(\mathbf{x}, \mathbf{y})$ and $\boldsymbol{\sigma}^i = \boldsymbol{\sigma}^i(\mathbf{x}, \mathbf{y})$ are defined on $S \times \mathbb{R}^2$ and are Y-periodic with respect to $\mathbf{y}$. Inserting these expansions into (51)-(52) and following the same procedure as for the in-plane case, one first gets $\operatorname{grad}_{\mathbf{y}} u^0 = 0$ in Y_m and hence

$$u^0(\mathbf{x}, \mathbf{y}) = U^0(\mathbf{x}) \quad \text{in} \quad S \times Y_m. \tag{55}$$

Then equation of motion (52) gives at order -1

$$\operatorname{div}_{\mathbf{y}}\boldsymbol{\sigma}^0 = \mathbf{0} \quad \text{in} \quad S \times Y$$

whereas the constitutive equation (51) gives at order 0

$$\boldsymbol{\sigma}^0 = \begin{cases} \mu_m\left(\operatorname{grad}_{\mathbf{x}} U^0 + \operatorname{grad}_{\mathbf{y}} u^1\right) & \text{in} \quad S \times Y_m \\ \mathbf{0} & \text{in} \quad S \times Y_f \end{cases}$$

One deduces by linearity that u^1 can be written in Y_m as

$$u^1(\mathbf{x}, \mathbf{y}) = \sum_{i=1}^2 \frac{\partial U^0}{\partial x_i}(\mathbf{x})\chi^i(\mathbf{y}) + U^1(\mathbf{x}) \quad \text{in} \quad S \times Y_m, \tag{56}$$

where χ^i, for $i = 1, 2$, are the out-of-plane displacement fields solutions of the elementary cell problems:

$$\begin{cases} \Delta_{\mathbf{y}}\chi^i = 0 & \text{in} \quad Y_m \\ (\mu_m\operatorname{grad}_{\mathbf{y}}\chi^i + \mathbf{e}_i)\cdot\mathbf{n} = 0 & \text{on} \quad \partial Y_f \\ \chi^i \quad \text{periodic}, \quad \mu_m\operatorname{grad}_{\mathbf{y}}\chi^i\cdot\mathbf{n} \quad \text{anti-periodic} & \text{on} \quad \partial Y \end{cases} \tag{57}$$

Therefore the stress field $\boldsymbol{\sigma}^0$ can read as

$$\boldsymbol{\sigma}^0(\mathbf{x}, \mathbf{y}) = \begin{cases} \displaystyle\sum_{i=1}^2 \mu_m\left(\operatorname{grad}_{\mathbf{y}}\chi^i(\mathbf{y}) + \mathbf{e}_i\right)\frac{\partial U^0}{\partial x_i}(\mathbf{x}) & \text{in} \quad S \times Y_m \\ \mathbf{0} & \text{in} \quad S \times Y_f \end{cases} . \tag{58}$$

14

3.2.2 Out-of-plane eigenvibrations of the inclusion fixed at its boundary

An out-of-plane eigenmode $\eta_* \neq 0$ and the associated eigenfrequency ω_* are solution of

$$\begin{cases} \mu_f \Delta_{\mathbf{y}} \eta_* + \rho_f \omega_*^2 \eta_* = 0 & \text{in} \quad Y_f \\ \eta_* = 0 & \text{on} \quad \partial Y_f \end{cases}. \tag{59}$$

As for the in-plane problem: (i) there exists a countable family of eigenfrequencies; (ii) the eigenmodes associated to an eigenfrequency constitute a linear space of finite dimension; (iii) the family of all the eigenmodes constitutes an orthogonal basis (in the sense of $L^2(Y_f)$ inner product) of the space of smooth out-of-plane displacement fields defined in Y_f and vanishing on ∂Y_f.

In our case of a circular inclusion, that eigenvalue problem can be solved in closed form. For every $p \in \mathbb{N}$, there exists a countable family of eigenfrequencies ω_* which are solutions of

$$J_p(k_*^s R) = 0, \qquad k_*^s = \frac{\omega_*}{c_s}. \tag{60}$$

The associated eigenmodes expressed in polar coordinates are

$$\eta_*(\mathbf{y}) = J_p(k_*^s r)(a_* \cos p\vartheta + b_* \sin p\vartheta) \tag{61}$$

where a_* and b_* are arbitrary constants (with $a_* \neq 0$ when $p = 0$, and $(a_*, b_*) \neq (0,0)$ when $p \neq 0$). As far as the property of orthogonality of the eigenmodes with respect to the constants (which correspond to the translations in the direction $\mathbf{e}_3$) is concerned, one must distinguish the case $p = 0$ from the other ones.

(i) When $p \neq 0$, the eigenmodes are orthogonal to the constants, *i.e.* the following equality holds true:

$$\int_{Y_f} \eta_*(\mathbf{y}) d\mathbf{y} = 0.$$

(ii) When $p = 0$, then the eigenmodes are purely radial and not orthogonal to the constants. Indeed, by virtue of (59)-(60), one has

$$\int_{Y_f} \eta_*(\mathbf{y}) d\mathbf{y} = a_* \pi \int_0^R r J_0(k_*^s r) dr = -\frac{a_* \pi R}{k_*^s} J_0'(k_*^s R) \neq 0,$$

the last inequality being due to the fact that $J_0'(x) \neq 0$ when $J_0(x) = 0$.

Accordingly, when $p = 0$, there exists a sequence of eigenfrequencies $\omega_n, n \in \mathbb{N}^*$, which can be expressed as

$$\omega_n = z_n \frac{c_s}{R} \tag{62}$$

where z_n are the roots of $J_0(z) = 0$:

$$z_1 = 2.4048, \quad z_2 = 5.5201, \quad z_3 = 8.6537, \quad z_4 = 11.7915, \cdots.$$

Let us note that, unlike the in-plane case, these z_n's are independent from ν_f.

3.2.3 The out-of-plane motion problem for the soft inclusion

In the inclusion, the homogenized first order displacement u^0 must satisfy the following local problem :

$$\begin{cases} \mu_f \Delta_{\mathbf{y}} u^0 + \rho_f \omega^2 u^0 = 0 & \text{in} \quad S \times Y_f \\ u^0 = U^0 & \text{on} \quad S \times \partial Y_f \end{cases} \tag{63}$$

For a given U^0 and a given ω which does not satisfy (60), problem (63) admits as unique solution u^0 that can be expressed as

$$u^0(\mathbf{x}, \mathbf{y}) = U^0(\mathbf{x}) \eta(\mathbf{y}) \quad \text{in} \quad S \times Y_f \tag{64}$$

where η is the solution of:

$$\begin{cases} \Delta \eta + (k^s)^2 \eta = 0 & \text{in} \quad Y_f \\ \eta = 1 & \text{on} \quad \partial Y_f \end{cases} \tag{65}$$

In the case of a circular inclusion, (65) can be solved in closed form and η reads

$$\eta(\mathbf{y}) = \frac{J_0(k^s r)}{J_0(k^s R)} \quad \text{with} \quad r = \|\mathbf{y}\| < R. \tag{66}$$

In the case where ω is an eigenfrequency ω_*, but with $J_0(k_*^s R) \neq 0$ (hence associated with an eigenmode number $p \neq 0$), the solution of (65) is defined up to an eigenmode and reads as

$$\eta(\mathbf{y}) = \frac{J_0(k_*^s r)}{J_0(k_*^s R)} + J_p(k_*^s r)(a_* \cos p\vartheta + b_* \sin p\vartheta), \tag{67}$$

where a_* and b_* are arbitrary constants.

In the case where ω is an eigenfrequency ω_* such that $J_0(k_*^s R) = 0$ (hence associated with a radial eigenmode), the problem (65) has no solution and the problem (63) has a solution only if $U^0 = 0$.

3.2.4 The effective out-of-plane motion problem for the composite

As explained in Section 3.1.2, the integration over the cell of the equation of motion gives at the order 0 an effective equation of motion (see (46)). Similarly, for out-of-plane polarized waves, that equation becomes

$$\text{div}\left(\mathbf{M}^* \text{grad} \, U^0\right) + \rho^{**}(\omega) \omega^2 U^0 = 0 \quad \text{in} \quad S \tag{68}$$

where $\mathbf{M}^*$ denotes the second order (out-of-plane) effective stiffness tensor whose components are given by

$$M_{ij}^* = \frac{1}{|Y|} \int_{Y_m} \mu_m \left(\text{grad}_{\mathbf{y}} \chi^i + \mathbf{e}_i\right) \cdot \left(\text{grad}_{\mathbf{y}} \chi^j + \mathbf{e}_j\right) d\mathbf{y}, \tag{69}$$

and $\rho^{**}(\omega)$ denotes the out-of-plane effective mass density given by

$$\rho^{**}(\omega) = \rho_m \frac{|Y_h|}{|Y|} + \frac{\rho_f}{|Y|} \int_{Y_f} \eta(\mathbf{y}) d\mathbf{y}. \tag{70}$$

In the case of a circular inclusion, $\rho^{**}(\omega)$ is obtained in closed form. Using (66) and (67), one gets

$$\rho^{**}(\omega) = \rho_{st} + \rho_f \frac{|Y_f|}{|Y|} \frac{J_2(k^s R)}{J_0(k^s R)}. \tag{71}$$

So, $\rho^{**}(\omega)$ is not defined when ω is equal to some ω_n defined by (62), and tends to $+\infty$ (resp. $-\infty$) when ω tends to ω_n from below (resp. from above). Accordingly, there exists a band gap $\tilde{I}_n$ of the form

$$\tilde{I}_n = \left[z_n \frac{c_s}{R}, \varphi_n\right], \quad n \in \mathbb{N}^*, \tag{72}$$

where φ_n are the frequencies corresponding to $\rho^{**} = 0$. Those band gaps can be seen in Figure 8.

16
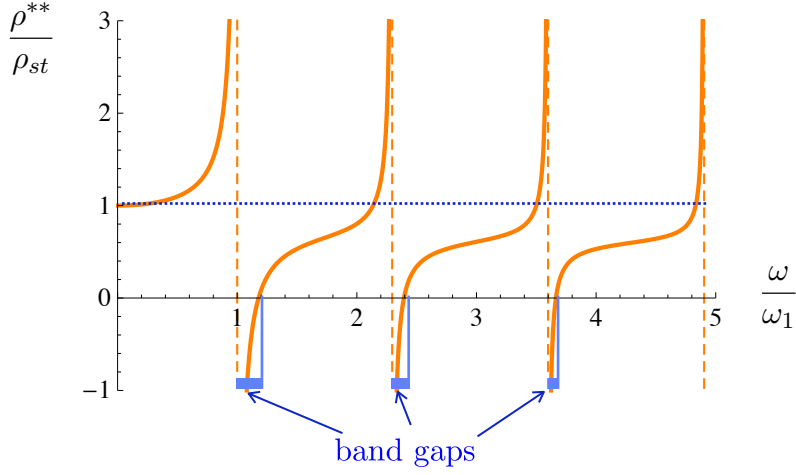
Fig. 8 Normalized effective mass vs. normalized frequency for out-of-plane polarized waves. The intervals of negative effective mass give the band gaps. The mass ratio between matrix and inclusion is 1.41 and corresponds to the material considered in Section 5.

4 Bloch-Floquet approach

4.1 Setting of the problem

The fundamental problem, denoted here below by $\mathcal{P}(\mathbf{k})$, consists in finding, for a given wave vector $\mathbf{k}$, a non trivial (complex) displacement field u, the associated (complex) stress field s and a frequency ω such that

$$
\mathcal{P}^\epsilon(\mathbf{k}) \quad
\begin{cases}
\operatorname{div} \mathsf{s} + \rho^\epsilon \omega^2 \mathsf{u} = 0 & \text{in} \quad Y^\epsilon \\
\mathsf{s} = \mathbf{E}^\epsilon \boldsymbol{\varepsilon}(\mathsf{u}) & \text{in} \quad Y^\epsilon \\
2\boldsymbol{\varepsilon}(\mathsf{u}) = \operatorname{grad} \mathsf{u} + \operatorname{grad} \mathsf{u}^T & \text{in} \quad Y^\epsilon \\
\mathsf{u}(\mathbf{x} + \mathbf{a}_i) = \exp(\mathrm{i}\,\mathbf{k} \cdot \mathbf{a}_i)\mathsf{u}(\mathbf{x}) & \forall \mathbf{x} \text{ on } \partial_i^- Y^\epsilon, i = 1, 2 \\
\mathsf{s}(\mathbf{x} + \mathbf{a}_i)\mathbf{n} = \exp(\mathrm{i}\,\mathbf{k} \cdot \mathbf{a}_i)\mathsf{s}(\mathbf{x})\mathbf{n} & \forall \mathbf{x} \text{ on } \partial_i^- Y^\epsilon, i = 1, 2
\end{cases}
$$

Here above, $\partial_i^- Y^\epsilon$ and $\partial_i^+ Y^\epsilon$ denote the opposite sides of the cell Y^ϵ in the direction i. Accordingly, one has

$$
\partial_i^+ Y^\epsilon = \partial_i^- Y^\epsilon + \mathbf{a}_i.
$$

Moreover, if $\mathbf{n}$ is the outer unit normal to $\partial_i^+ Y^\epsilon$, then $-\mathbf{n}$ is the outer unit normal to $\partial_i^- Y^\epsilon$.

The main goal is to find the spectrum, that is to say, the set described by the frequencies when the wave vector $\mathbf{k}$ describes $\mathbb{R}^2$.

By a change of variable, the problem can be reformulated in order to work with periodic fields. Specifically, introducing $\hat{\mathsf{u}}$ by

$$
\mathsf{u}(\mathbf{x}) = \exp(\mathrm{i}\,\mathbf{k} \cdot \mathbf{x})\hat{\mathsf{u}}(\mathbf{x}), \qquad \forall \mathbf{x} \in Y^\epsilon,
$$

the problem consists now in finding a non trivial displacement field $\hat{\mathsf{u}}$, the associated stress field $\hat{\mathsf{s}}$ and a frequency ω such that

$$
\hat{\mathcal{P}}^\epsilon(\mathbf{k}) \quad
\begin{cases}
\operatorname{div} \hat{\mathsf{s}} + \mathrm{i}\,\hat{\mathsf{s}}\,\mathbf{k} + \rho^\epsilon \omega^2 \hat{\mathsf{u}} = 0 & \text{in} \quad Y^\epsilon \\
\hat{\mathsf{s}} = \mathbf{E}^\epsilon\big(\boldsymbol{\varepsilon}(\hat{\mathsf{u}}) + \mathrm{i}\hat{\mathsf{u}} \odot \mathbf{k}\big) & \text{in} \quad Y^\epsilon \\
\hat{\mathsf{u}} \text{ periodic and } \hat{\mathsf{s}}\mathbf{n} \text{ anti-periodic} & \text{on } \partial Y^\epsilon
\end{cases} \tag{73}
$$

17

The fundamental problem can be written in a variational form. Indeed, let us introduce, for a given wave vector $\mathbf{k}$, the Rayleigh ratio $\mathcal{R}_{\mathbf{k}}$ defined on the space $\mathsf{H}^1_{\#}(Y^\epsilon)$ of (complex) fields which are in $\mathsf{H}^1(Y^\epsilon)$ and Y^ϵ-periodic:

$$\mathcal{R}_{\mathbf{k}}(\hat{\mathbf{v}}) = \frac{\displaystyle\int_{Y^\epsilon} \mathbf{E}^\epsilon(\boldsymbol{\varepsilon}(\hat{\mathbf{v}}) + i\hat{\mathbf{v}} \odot \mathbf{k}) \cdot (\boldsymbol{\varepsilon}(\bar{\hat{\mathbf{v}}}) - i\bar{\hat{\mathbf{v}}} \odot \mathbf{k})d\mathbf{x}}{\displaystyle\int_{Y^\epsilon} \rho^\epsilon \left|\hat{\mathbf{v}}\right|^2 d\mathbf{x}}. \tag{74}$$

The following proposition holds true:

Proposition 1 *The displacement fields $\hat{\mathbf{u}}$ solution of $\hat{\mathcal{P}}^\epsilon(\mathbf{k})$ are the stationary points of the Rayleigh ratio $\mathcal{R}_{\mathbf{k}}$ and the associated frequencies ω are given by the Rayleigh ratio of $\hat{\mathbf{u}}$,*

$$\mathcal{R}'_{\mathbf{k}}(\hat{\mathbf{u}})(\hat{\mathbf{v}}) = 0 \quad \forall \hat{\mathbf{v}} \in \mathsf{H}^1_{\#}(Y^\epsilon), \qquad \omega^2 = \mathcal{R}_{\mathbf{k}}(\hat{\mathbf{u}}), \tag{75}$$

where $\mathcal{R}'_{\mathbf{k}}(\hat{\mathbf{u}})(\hat{\mathbf{v}})$ stands for the directional derivative of $\mathcal{R}_{\mathbf{k}}$ at $\hat{\mathbf{u}}$ in the direction $\hat{\mathbf{v}}$.

The proof is classical and we only gives the main lines. First, taking the derivative of $\mathcal{R}_{\mathbf{k}}$, the stationary condition reads as

$$\int_{Y^\epsilon} \mathbf{E}^\epsilon(\boldsymbol{\varepsilon}(\hat{\mathbf{u}}) + i\hat{\mathbf{u}} \odot \mathbf{k}) \cdot (\boldsymbol{\varepsilon}(\bar{\hat{\mathbf{v}}}) - i\bar{\hat{\mathbf{v}}} \odot \mathbf{k})d\mathbf{x} = \omega^2 \int_{Y^\epsilon} \rho^\epsilon \hat{\mathbf{u}} \cdot \bar{\hat{\mathbf{v}}}d\mathbf{x}, \quad \forall \hat{\mathbf{v}} \in \mathsf{H}^1_{\#}(Y^\epsilon). \tag{76}$$

Using the definition of $\hat{\mathbf{s}}$, (76) becomes

$$\int_{Y^\epsilon} \hat{\mathbf{s}} \cdot (\boldsymbol{\varepsilon}(\bar{\hat{\mathbf{v}}}) - i\bar{\hat{\mathbf{v}}} \odot \mathbf{k})d\mathbf{x} = \omega^2 \int_{Y^\epsilon} \rho\hat{\mathbf{u}} \cdot \bar{\hat{\mathbf{v}}}d\mathbf{x}, \quad \forall \hat{\mathbf{v}} \in \mathsf{H}^1_{\#}(Y^\epsilon).$$

Making an integration by parts of the term $\hat{\mathbf{s}} \cdot \boldsymbol{\varepsilon}(\bar{\hat{\mathbf{v}}})$ above and using the fact that $\hat{\mathbf{v}}$ is arbitrary in $\mathsf{H}^1_{\#}(Y^\epsilon)$, one gets by standard arguments of Calculus of Variations that $\hat{\mathbf{s}}$ satisfies the equation of motion in Y^ϵ and $\hat{\mathbf{s}}\mathbf{n}$ is anti-periodic on ∂Y^ϵ. Hence, $\hat{\mathbf{u}}$, $\hat{\mathbf{s}}$ and ω are solution of $\hat{\mathcal{P}}^\epsilon(\mathbf{k})$. One proves the converse in the same manner.

4.2 Some general properties

Let us first indicate some general properties of the fundamental Bloch-Floquet problem.

1. *The spectral theorem.* Using the variational formulation of the fundamental problem, one gets the so-called spectral theorem:

   Proposition 2 (Spectral theorem) *At given $\mathbf{k}$, the solutions of $\hat{\mathcal{P}}^\epsilon(\mathbf{k})$ enjoy the following properties:*
   (a) The eigen-frequencies ω constitute a sequence of real numbers ω_n, $n \in \mathbb{N}$, which tends to infinity without accumulation points;
   (b) The eigen-displacement fields associated with an eigen-frequency ω_n constitute a subspace $\mathcal{U}_n$ of $\mathsf{H}^1_{\#}(Y^\epsilon)$ of finite dimension;
   (c) The eigen-spaces are orthogonal to each other in the sense of the scalar product

$$(\hat{\mathbf{u}}, \hat{\mathbf{v}}) = \int_{Y^\epsilon} \rho^\epsilon \hat{\mathbf{u}} \cdot \bar{\hat{\mathbf{v}}}d\mathbf{x}$$

   and constitute a countable basis of $\mathsf{H}^1_{\#}(Y^\epsilon)$.

The proof is a variant of the classical one for self-adjoint compact operators, see [13]. It is based on the minimization of the Rayleigh ratio.

2. *Periodic dependence of ω on $\mathbf{k}$.* It is easy to verify that if $\hat{\mathsf{u}}$, $\hat{\mathsf{s}}$ and ω are solution of the problem $\hat{\mathcal{P}}^\epsilon(\mathbf{k})$, then they are also solution of the problem $\hat{\mathcal{P}}^\epsilon(\mathbf{k} + \mathbf{A})$ for all $\mathbf{A}$ such that

$$\mathbf{A} = p\mathbf{A}_1 + q\mathbf{A}_2 \quad \text{with} \quad p, q \in \mathbb{N}.$$

where $\mathbf{A}_i$ are the basis vectors of the reciprocal lattice, see Figure 1d. The proof is essentially based on the fact that $\exp(i\mathbf{A} \cdot \mathbf{a}_1) = \exp(i\mathbf{A} \cdot \mathbf{a}_2) = 1$. Consequently, one can restrict the study of the spectrum to the wave vectors $\mathbf{k}$ lying in the First Brillouin Zone (BZ).

3. *Smooth dependence of the solution of $\hat{\mathcal{P}}^\epsilon(\mathbf{k})$ on $\mathbf{k}$.* By using classical results on linear operators, one knows that the solution of $\hat{\mathcal{P}}^\epsilon(\mathbf{k})$, and hence the frequency ω, depends smoothly (in fact is a C^∞ function) of the wave vector $\mathbf{k}$.

4. $\omega = 0$ *is always solution of $\hat{\mathcal{P}}^\epsilon(\mathbf{0})$.* Indeed, taking $\mathbf{k} = \mathbf{0}$, one easily checks that $\hat{\mathsf{u}}(\mathbf{x}) = \hat{\mathsf{U}}$ (a constant), $\hat{\mathsf{s}} = \mathbf{0}$ and $\omega = 0$ are solution of $\hat{\mathcal{P}}^\epsilon(\mathbf{0})$. The eigen-space $\mathcal{U}_0$ corresponds to the translations (the rotations are forbidden by the periodic conditions).

5. $\omega = 0$ *is not solution of $\hat{\mathcal{P}}^\epsilon(\mathbf{k})$ when $\mathbf{k} \in \mathrm{BZ}$, $\mathbf{k} \neq \mathbf{0}$.* Indeed, by virtue of the positivity of the Rayleigh ratio, in order that $\omega = 0$ be a minimizer of $\mathcal{R}_\mathbf{k}$, one must have $\mathcal{R}_\mathbf{k}(\hat{\mathsf{u}}) = 0$ and hence $\boldsymbol{\varepsilon}(\hat{\mathsf{u}}) + i\hat{\mathsf{u}} \odot \mathbf{k} = 0$. In terms of the original field u, one gets

$$\boldsymbol{\varepsilon}(\mathsf{u}) = \exp(i\mathbf{k} \cdot \mathbf{x})(\boldsymbol{\varepsilon}(\hat{\mathsf{u}}) + i\hat{\mathsf{u}} \odot \mathbf{k}) = 0.$$

Hence, u must be a rigid displacement field of the form $\mathsf{u}(\mathbf{x}) = \mathsf{U} + \mathsf{w} \wedge \mathbf{x}$. The boundary conditions $\mathsf{u}(\mathbf{x} + \mathbf{a}_i) = \exp(\mathbf{k} \cdot \mathbf{a}_i)\mathsf{u}(\mathbf{x})$ on $\partial_i^- Y^\epsilon$ requires that $\mathsf{w} = 0$ and $\mathsf{U} = \exp i\mathbf{k} \cdot \mathbf{a}_i\mathsf{U}$, for $i = 1, 2$. Therefore, one must have $\exp i\mathbf{k} \cdot \mathbf{a}_i = 1$ for $i = 1, 2$ which is possible only if $\mathbf{k} = \mathbf{0}$.

6. *There is no band gap in the neighborhood of $\omega = 0$.* Indeed $\omega = 0$ is solution when $\mathbf{k} = \mathbf{0}$ but not when $\mathbf{k} \neq \mathbf{0}$. If one considers the frequency which minimizes the Rayleigh ratio $\mathcal{R}_\mathbf{k}$, say $\omega_0(\mathbf{k})$, since it depends continuously on $\mathbf{k}$ and since

$$\omega_0(\mathbf{k}) \begin{cases} = 0 & \text{if } \mathbf{k} = \mathbf{0} \\ > 0 & \text{if } \mathbf{k} \neq \mathbf{0} \end{cases},$$

there exists a neighborhood of 0 in which all the frequencies can be reached.

7. *Dependence of the spectrum on the size of the cell.* Let us change the cell Y^ϵ by λY^ϵ (homothetic transformation by the ratio $\lambda > 0$) and the wave vector $\mathbf{k}$ by $\mathbf{k}/\lambda$. If $\hat{\mathsf{u}}$ and ω are solution of the problem $\hat{\mathcal{P}}^\epsilon(\mathbf{k})$ associated with the cell Y^ϵ, then $\hat{\mathsf{u}}_\lambda$ defined on λY^ϵ by $\hat{\mathsf{u}}_\lambda(\mathbf{x}) = \hat{\mathsf{u}}(\mathbf{x}/\lambda)$ and $\omega_\lambda = \omega/\lambda$ are solution of the problem $\hat{\mathcal{P}}^\epsilon(\mathbf{k}/\lambda)$ associated with the cell λY^ϵ. Therefore, the spectrum associated with λY^ϵ is obtained from that associated with Y^ϵ by the factor $1/\lambda$. In other words, a change of size does not modify the structure of the spectrum but simply changes the scale of the eigen-frequencies. In particular, the existence and the structure of band gaps remain unchanged by changing the size of the cell. To change the structure of the band gaps, one must change the materials inside the cell.

4.3 Rescaling

Since, by virtue of the above Property (7), the frequencies scale with the cell dimension, it is more convenient to consider the rescaled cell $Y = Y^\epsilon/\epsilon$ already introduced in Section 3.1.2, see Figure 2. Recalling the definition of the rescaled coordinate $\mathbf{y} = \mathbf{x}/\epsilon$, at $\hat{\mathsf{u}}$ and $\hat{\mathsf{s}}$ defined on Y^ϵ one can associate $\hat{\mathsf{u}}^\epsilon$ and $\hat{\mathsf{s}}^\epsilon$ defined on Y by

$$\hat{\mathsf{u}}^\epsilon(\mathbf{y}) = \hat{\mathsf{u}}(\epsilon\mathbf{y}), \qquad \hat{\mathsf{s}}^\epsilon(\mathbf{y}) = \hat{\mathsf{s}}(\epsilon\mathbf{y}).$$

Introducing these rescaling into $\hat{\mathcal{P}}^\epsilon(\mathbf{k})$ given in (73), the rescaled Bloch-Floquet problem consists in finding $\hat{\mathbf{u}}^\epsilon \neq 0$, $\hat{\mathbf{s}}^\epsilon$ and ω^ϵ such that

$$
\hat{\mathsf{P}}^\epsilon(\mathbf{k})
\begin{cases}
\epsilon^{-1}\mathrm{div}\,\hat{\mathbf{s}}^\epsilon + \mathrm{i}\,\hat{\mathbf{s}}^\epsilon\,\mathbf{k} + \rho_f\,\omega^{\epsilon 2}\hat{\mathbf{u}}^\epsilon = 0 & \text{in} \quad Y_f \\
\hat{\mathbf{s}}^\epsilon = \epsilon\mathbf{E}_f\big(\boldsymbol{\varepsilon}(\hat{\mathbf{u}}^\epsilon) + \epsilon\mathrm{i}\hat{\mathbf{u}}^\epsilon \odot \mathbf{k}\big) & \text{in} \quad Y_f \\
\hat{\mathbf{u}}^\epsilon \text{ and } \hat{\mathbf{s}}^\epsilon\,\mathbf{n} \text{ continue} & \text{on} \quad \partial Y_f \\
\epsilon^{-1}\mathrm{div}\,\hat{\mathbf{s}}^\epsilon + \mathrm{i}\,\hat{\mathbf{s}}^\epsilon\,\mathbf{k} + \rho_m\,\omega^{\epsilon 2}\hat{\mathbf{u}}^\epsilon = 0 & \text{in} \quad Y_m \\
\hat{\mathbf{s}}^\epsilon = \epsilon^{-1}\mathbf{E}_m\big(\boldsymbol{\varepsilon}(\hat{\mathbf{u}}^\epsilon) + \epsilon\mathrm{i}\hat{\mathbf{u}}^\epsilon \odot \mathbf{k}\big) & \text{in} \quad Y_m \\
\hat{\mathbf{u}}^\epsilon \text{ periodic and } \hat{\mathbf{s}}^\epsilon\mathbf{n} \text{ anti-periodic} & \text{on } \partial Y
\end{cases}
\tag{77}
$$

where we distinguish between the two constituents materials. In the equations above, all the derivatives are taken with respect to $\mathbf{y}$. Note that the frequency has not been rescaled, ω^ϵ represents the "true" angular frequency of the "true" cell Y^ϵ.

In the next subsection, we make an asymptotic analysis of this rescaled Bloch-Floquet problem by considering in-plane wave vectors $\mathbf{k}$ and we compare the results with the homogenization approach.

4.4 Asymptotic analysis of $\hat{\mathsf{P}}^\epsilon(\mathbf{k})$ at given $\mathbf{k}$.

One considers an in-plane wave vector $\mathbf{k} = k_1\mathbf{e}_1 + k_2\mathbf{e}_2$ and searches for solutions which admit the following expansions in terms of ϵ:

$$
\begin{cases}
\hat{\mathbf{u}}^\epsilon = \hat{\mathbf{u}}^0 + \epsilon\hat{\mathbf{u}}^1 + \cdots, & \hat{\mathbf{u}}^0 \neq 0, \\
\hat{\mathbf{s}}^\epsilon = \hat{\mathbf{s}}^0 + \epsilon\hat{\mathbf{s}}^1 + \cdots \\
\omega^\epsilon = \omega + \cdots
\end{cases}
$$

where we have omitted the superscript 0 for the leading term of the frequency expansion, to simplify the notation. In the expansion above, the displacements and the stresses are three-dimensional (with in-plane and out-of-plane components) but these components depend only on (y_1, y_2).

– Inserting those expansions into $\hat{\mathsf{P}}^\epsilon(\mathbf{k})$ given in (77), the constitutive relation at order -1 reads $\boldsymbol{\varepsilon}(\hat{\mathbf{u}}^0) = 0$ in Y_m and hence

$$
\hat{\mathbf{u}}^0(\mathbf{y}) = \mathsf{U}^0 \quad \text{in} \quad Y_m,
\tag{78}
$$

U^0 being an arbitrary (three-dimensional) vector.
– The constitutive equations in Y_m and Y_f give at order 0

$$
\hat{\mathbf{s}}^0 =
\begin{cases}
\mathbf{0} & \text{in } Y_f \\
\mathbf{E}_m\big(\boldsymbol{\varepsilon}(\hat{\mathbf{u}}^1) + \mathrm{i}\mathsf{U}^0 \odot \mathbf{k}\big) & \text{in } Y_m
\end{cases}
\tag{79}
$$

whereas the equation of motion in Y_m at order -1 reads

$$
\mathrm{div}\hat{\mathbf{s}}^0 = 0 \quad \text{in} \quad Y_m.
$$

Therefore, using the results of the Section 3, $\hat{\mathbf{u}}^1$ can be written in the following form

$$
\hat{\mathbf{u}}^1(\mathbf{y}) = \mathrm{i}\sum_{i,j=1}^{2} \mathsf{U}_i^0 k_j \boldsymbol{\chi}^{ij}(\mathbf{y}) + \mathrm{i}\sum_{i,j=1}^{2} \mathsf{U}_3^0 k_j \chi^i(\mathbf{y})\mathbf{e}_3 + \mathsf{U}^1 \quad \text{in} \quad Y_m
\tag{80}
$$

where the vectors $\boldsymbol{\chi}^{ij}$ are the solutions of the elementary in-plane cell problems (13), the scalars χ^i are the solutions of the elementary out-of-plane cell problems (57) and U^1 is an arbitrary (three-dimensional) vector.

– In Y_f, using the previous results, the constitutive equation at order 1 and the equation of motion at order 0 lead to the following problem for $\hat{\mathsf{u}}^0$:

$$\begin{cases} \mathrm{div}\hat{\mathsf{s}}^1 + \rho_f\omega^2\hat{\mathsf{u}}^0 = \mathbf{0} & \text{in } Y_f \\ \hat{\mathsf{s}}^1 = \mathbf{E}_f\varepsilon(\hat{\mathsf{u}}^0) & \text{in } Y_f \\ \hat{\mathsf{u}}^0 = \mathsf{U}^0 & \text{on } \partial Y_f \end{cases} \tag{81}$$

which is a linear combination of The in-plane and out-of-plane problems (32) and (63). Indeed, by linearity (81) can be decomposed into a plane strain problem where $\hat{\mathsf{u}}^0_3 = \mathsf{U}^0_3 = 0$ and into an antiplane strain problem where $\hat{\mathsf{u}}^0_i = \mathsf{U}^0_i = 0$ for $i = 1,2$. Therefore, one can use all the results from Section 3.1.4 up to Section 3.1.6 for the in plane problem, and from Section 3.2.3 to Section 3.2.4 for the out-of-plane problem.

– The equation of motion in the whole cell at order 0 reads as

$$\mathrm{div}\hat{\mathsf{s}}^1 + i\hat{\mathsf{s}}^0\mathbf{k} + \rho\omega^2\hat{\mathsf{u}}^0 = 0 \quad \text{in} \quad Y.$$

Integrating that equation over Y and using the periodic boundary condition give the following equation:

$$i\langle\hat{\mathsf{s}}^0\rangle\mathbf{k} + \omega^2\langle\rho\hat{\mathsf{u}}^0\rangle = 0. \tag{82}$$

Using (79)–(81), (82) becomes

$$\begin{cases} \text{for } i = 1,2, \quad \displaystyle\sum_{j,p,q=1}^{2}\left(E^*_{ijpq}k_jk_q - \rho^*_{ip}(\omega)\omega^2\right)\mathsf{U}^0_p = 0 \\ \text{for } i = 3, \quad \displaystyle\sum_{j,q=1}^{2}\left(M^*_{jq}k_jk_q - \rho^{**}(\omega)\omega^2\right)\mathsf{U}^0_3 = 0 \end{cases} \tag{83}$$

where $\mathbf{E}^*$ is the effective in-plane stiffness tensor given by (16), $\boldsymbol{\rho}^*(\omega)$ is the effective in-plane mass density given by (44), $\mathbf{M}^*$ is the effective out-of-plane stiffness tensor given by (69) and $\rho^{**}(\omega)$ is the effective out-of-plane mass density given by (70). In the case of a circular inclusion, $\boldsymbol{\rho}^*(\omega) = \rho^*(\omega)\mathbf{I}$ with $\rho^*(\omega)$ given by (47) whereas $\rho^{**}(\omega)$ is given by (71). So, we have found the same equations as in the homogenization approach. The end of the discussion to find the spectrum is essentially the same as in Section 3. We finally recover that the band gaps are the intervals I_n and $\tilde{I}_n$, $n \in \mathbb{N}^*$, defined in Section 3, see (48) and (72).

5 Examples

The above results are illustrated in this section with reference to a 2D periodic material, characterized by a square elementary cell of side a constituted by an aluminium matrix with polymeric cylindrical inclusions of radius $R = 0.415a$, Figure 9a. The reciprocal lattice vectors $\mathbf{A}_1$ and $\mathbf{A}_2$ are equal and orthogonal, and the First Brillouin Zone is also a square. Figure 9b shows the Wigner-Seitz cell of the reciprocal lattice with the shaded triangle representing, account taken of the symmetries, the Irreducible Brillouin Zone (IBZ). In the following numerical analyses only wave vectors belonging to the boundary of the IBZ, along the path $\Gamma - X - M - \Gamma$ will be considered as proposed e.g. in [20].
The properties of the constituents are given in Table 2.
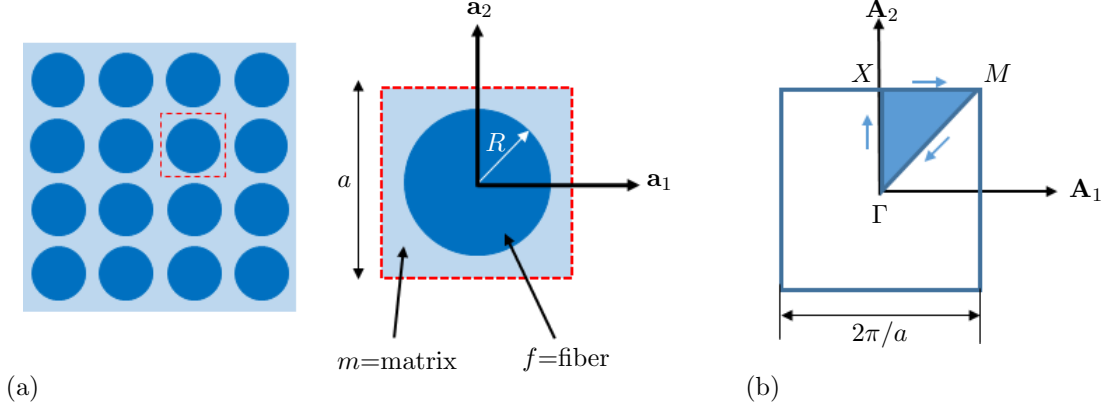
Fig. 9 2D periodic material, PVC inclusions in aluminium matrix: (a) material lattice and elementary cell, (b) reciprocal lattice and IBZ (shaded area).

Constituent	λ [MPa]	μ [MPa]	ρ [Kg/m^3]
matrix (Al)	57375.	27000.	2500.
fiber (PVC)	160.	40.	1500.

Table 2 Material properties

5.1 In-plane waves

The homogenization approach is based on the hypotheses listed in Section 2. In particular hypothesis (3) can be rewritten as

$$\begin{cases} \dfrac{a}{L_m} = a\omega\sqrt{\dfrac{\rho_m}{\lambda_m + 2\mu_m}} << 1 \text{ for longitudinal waves} \\[3mm] \dfrac{a}{L_m} = a\omega\sqrt{\dfrac{\rho_m}{\mu_m}} << 1 \text{ for shear waves} \end{cases} \tag{84}$$

meaning that the homogenization approach, for a given material, applies only to waves with low frequencies, i.e. waves with $\omega << \omega_{max} = \sqrt{\frac{\mu_m}{\rho_m}}/a$. Therefore the prediction of the band gaps given by the homogenization approach is a reasonable estimate only if the corresponding frequencies given in eq. (48) are smaller than ω_{max}.

For the constituents listed in table 2, and $a = 1$ mm, $f_{max} = \frac{1}{2\pi}\omega_{max} = 523$ kHz while the opening and closing frequencies of the first band gap defined in (48) read, respectively,

$$\frac{1}{2\pi}\frac{\zeta_1}{R}\sqrt{\frac{\lambda_m + 2\mu_m}{\rho_f}} = 268\,\text{kHz} \quad \text{and} \quad \frac{\theta_1}{2\pi} = 291\,\text{kHz} \tag{85}$$

thus defining an interval verifying conditions (84).

Figure 10 shows the dispersion plot, numerically obtained by imposing the periodic Bloch-Floquet conditions on a unit cell, discretized by finite elements, and the plot of the effective mass ρ^* obtained through homogenization. For the sake of comparison, the latter is shown rotated of $\pi/2$, as reduced frequency vs effective mass density diagram. The shaded regions in Figure 10a correspond to band gaps; their relative amplitude, defined as the bandwidth divided by the central gap frequency, is also reported. Note that, in view of the Property 7. of Section 4.2, the dispersion plot in term of reduced frequency $\omega a/2\pi$, is independent from the cell size a. The shaded regions in Figure 10b correspond to the intervals of negative mass density. One can observe that the first band gap in the dispersion plot (Fig. 10a) exactly corresponds to the frequency range of negative effective mass (Fig. 10b); this is not the case for the second one, as it occurs at frequencies that do not satisfy hypothesis (3) in Section 2.

22
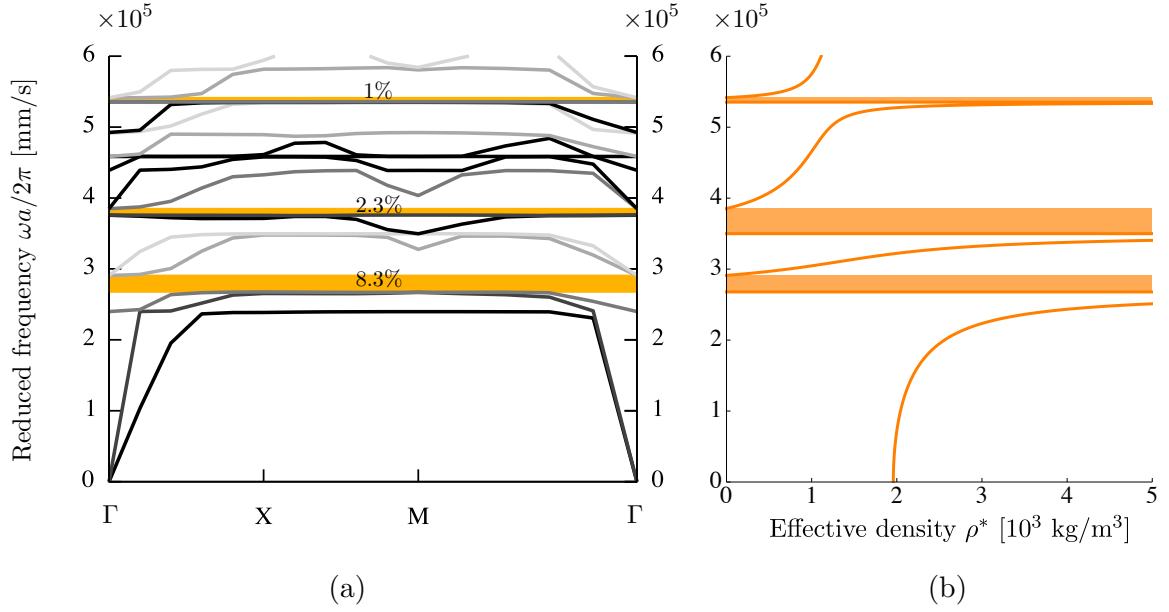
Fig. 10 2D periodic material, PVC inclusions in aluminium matrix, in-plane propagation: (a) dispersion plot with shaded bandgaps, (b) effective mass density vs reduced frequency, shaded areas correspond to negative effective mass.
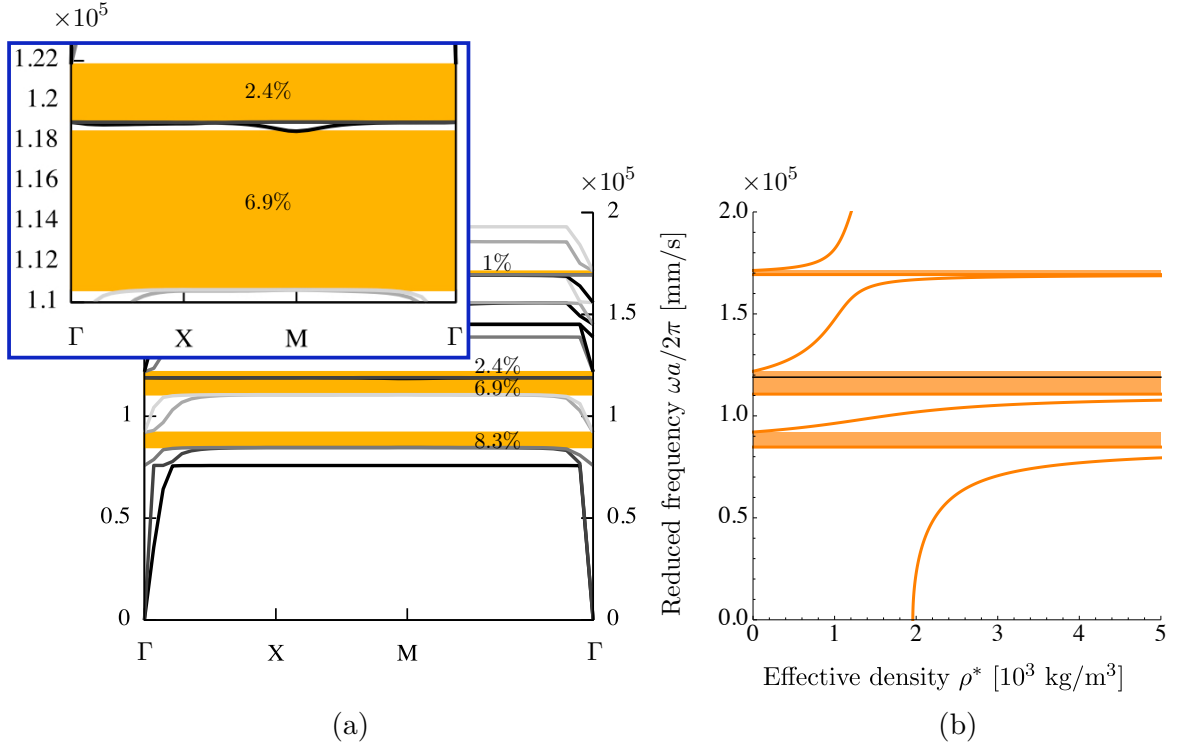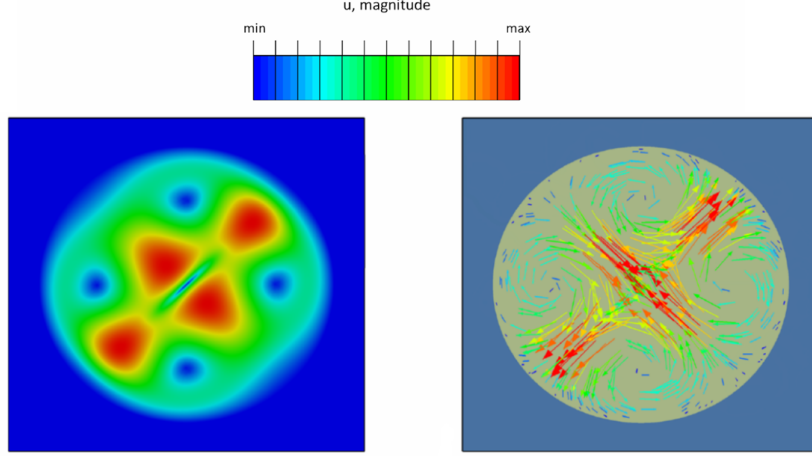

Fig. 11 2D periodic material, very soft inclusions in aluminium matrix, in-plane propagation: (a) dispersion plot with shaded bandgaps and with the inset representing a zoomed view of the second bandgap, (b) effective mass density vs reduced frequency, shaded areas correspond to negative effective mass.

The range of validity of the predictions given by the homogenization approach increases as the contrast between the stiffness of the two constituent materials increases. Let us consider for instance inclusions

characterized by elastic moduli of one tenth of those of PVC reported in Table 2. The corresponding dispersion plot is shown in Figure 11a, while Figure 11b reports the variation of the equivalent mass density with the frequency. In this case the first three zones of negative equivalent stiffness correspond to frequencies well below the maximum frequency $f_{max} = 523$ kHz which is set by the matrix properties, hence they give a good prediction of the first three band gaps numerically obtained. However the zoomed view of the dispersion plot shows that the second band gap, between 110.6 kHz and 121.8 kHz is actually separated into two smaller bandgaps (between 110.6 kHz and 118.5 kHz and between 119.0 kHz and 121.8 kHz) by two flat modes. These latter correspond to local resonances of the inclusion endowed with a displacement field inside the inclusion like a dipole, with almost zero displacements in the matrix as shown in Figure 12. These modes have already been evidenced in [22].

Fig. 12 2D periodic material, in-plane propagation, very soft inclusions in Aluminium matrix. Representation of the 6th flat eigenmode: (a) contour of the displacements modulus, (b) direction and amplitude of displacements vectors.

Actually the presence of these modes is also predicted by the present homogenization approach, they correspond to the eigenfrequency ω_n^p with $n = 1$ and $p = 2$ which, for the considered example, is equal to 118.98 kHz (black line in Figure 11b). This frequency turns out to fall inside the second interval of negative effective mass as shown by Figure 13 where the curve den_2 (in blue), whose zero gives ω_n^2, is superposed to the effective mass plot. On the same figure the curve den_1 is plotted by a dashed black line: the zero gives the frequencies $\omega_n^1 = \omega_1, \omega_2, \omega_3, ..$ which correspond to the band-gap opening.
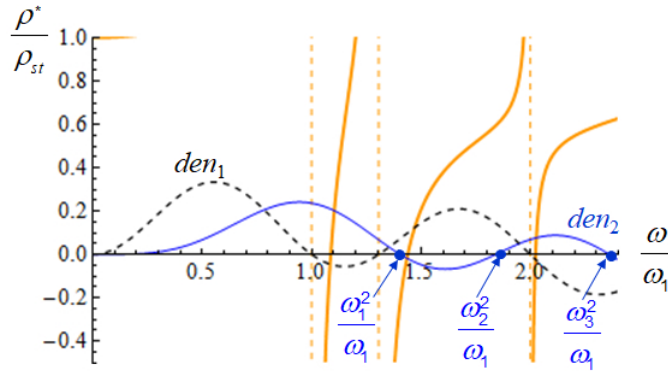
Fig. 13 Graphs of ρ^*/ρ_{st} in orange, den_1 in black, dashed and den_2 in blue for $\nu_f = 0.4$ and mass ratio between matrix and inclusion equal to 1.41.

24

5.2 Out-of-plane waves

Consider now the propagation of out-of-plane waves in the material with aluminium matrix and PVC inclusions. The first two intervals of frequencies leading to a negative effective mass, as defined in (44), are [150.6 kHz - 177.5 kHz] and [345.7 kHz - 360.5kHz]. Since for the constituents of Table 2, and $a = 1$ mm, the limit frequency is $f_{max} = \frac{1}{2\pi}\omega_{max} = 523$ kHz, both intervals are within the low frequency regime and hence give a good prediction of the first two bandgaps. This is confirmed by the comparison between the dispersion plot, numerically obtained by imposing the Bloch-Floquet conditions (Fig. 14a) and the effective mass plot obtained through homogenization (Fig. 14b).
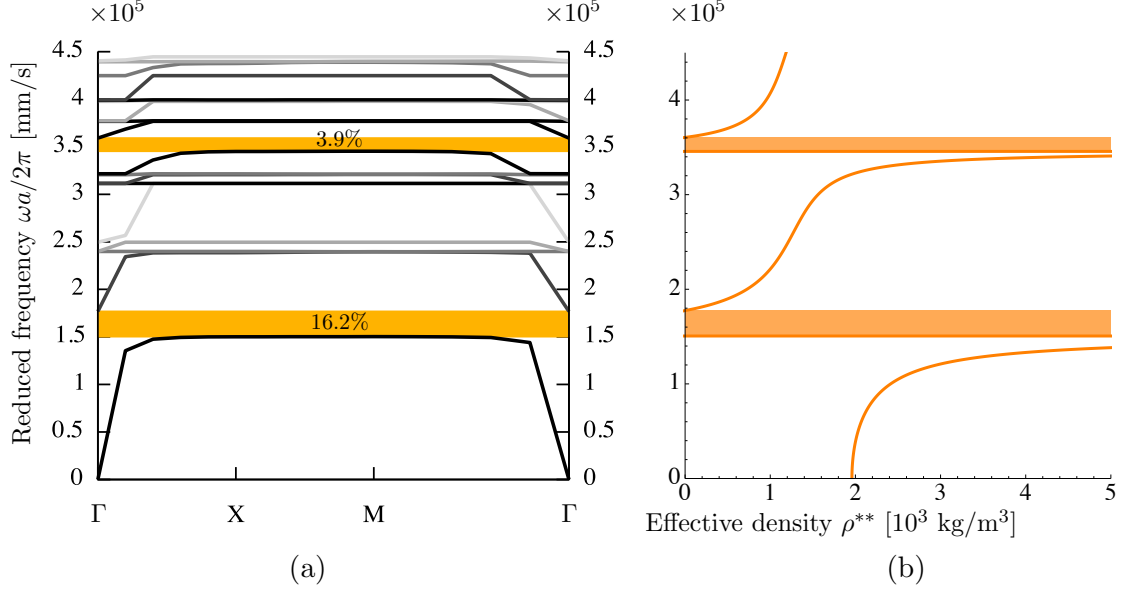
Fig. 14 2D periodic material, PVC inclusions in aluminium matrix, out-of-plane propagation: (a) dispersion plot with shaded bandgaps, (b) effective mass density vs reduced frequency, shaded areas correspond to negative effective mass.

6 Conclusions

In this paper, we have provided a detailed study of band gaps formation in 2D binary, locally resonant metamaterials. Under the hypothesis of soft inclusion in hard matrix, the problem has been tackled by two different approaches: the homogenization approach, based on the scale separation, and the Bloch-Floquet analysis. In the first case the band gaps are identified as the intervals of negative effective mass of the homogenized continuum, while in the second band gaps are identified as the frequency intervals where no real solution of the Bloch-Floquet problem exists.

The main findings, which are valid under the hypothesis of high contrast between the constituents and in the long wave length limit, can be summarized as follows:

– the two approaches are fully equivalent and provide the same band-gaps prediction;
– in the case of circular inclusion the intervals of negative effective mass density are computed in closed form both for in-plane and out of plane propagation;
– the opening frequency of the band gap only depends on the material and geometric properties of the inclusion;
– the closing frequency of the band gap also depends on the mass ratio between inclusion and matrix and increases as this ratio increases, thus leading to a wider band gap;

– the elastic properties of the matrix indirectly intervene through the hypotheses of validity of the approach, but do not intervene directly in the band gap limits;
– there exist some locally resonant modes that correspond to flat modes that can fall inside the band gaps.

All above results are illustrated through several examples on specific materials. A very good agreement between the numerical results of the analysis of dispersion with Bloch-Floquet boundary conditions and the analytical results obtained through homogenizations is obtained and the range of validity of the approach is confirmed.

It is worthnoting that the two scale homogenization adopted requires that the ratio between the stiffness of the inclusions and the stiffness of the matrix is of the order of ϵ^2, with ϵ very small. Actually numerical tests have shown that this approach leads to a very good prediction of the first bandgap, already for $\epsilon \approx 0.04$. The closed form expressions obtained are well suited for material optimization and design.

The present approach cannot be used to predict band gaps formation in composite materials with stiff inclusions in soft matrix, nor an extension seem feasible in this direction. On the contrary, the estension of the homogenization approach for band gaps prediction in ternary LRM (e.g. materials with hard inclusions with soft coating embedded in a stiff matrix) seems possible and is currently under study.

References

1. Åberg, M., Gudmundson, P.: The usage of standard finite element codes for computation of dispersion relations in materials with periodic microstructure. J. Acoust. Soc. Am. **102**(4), 2007–2013 (1997)
2. Allaire, G.: Homogenization and 2-scale convergence. SIAM J. Math. Anal. **23**(6), 1482–1518 (1992)
3. Allaire, G., Briane, M., Vanninathan, M.: A comparison between two-scale asymptotic expansions and Bloch wave expansions for the homogenization of periodic structures. SeMA Journal: Boletin de la Sociedad Española de Matemática Aplicada **73**(3), 237–259 (2016)
4. Antonakakis, T., Craster, R.V., Guenneau, S.: Homogenisation for elastic photonic crystals and dynamic anisotropy. J. Mech. Phys. Solids **71**(1), 84–96 (2014)
5. Auriault, J.L., Bonnet, G.: Dynamique des composites élastiques périodiques. Arch.Mech. **37**(January 1985), 269–284 (1985)
6. Auriault, J.L., Boutin, C.: Long wavelength inner-resonance cut-off frequencies in elastic composite materials. Int. J. Solids Struct. **49**(23-24), 3269–3281 (2012)
7. Brillouin, L.: Wave propagation in periodic structures. Dover, New York (1953)
8. Colombi, A., Roux, P., Guenneau, S., Gueguen, P., Craster, R.V.: Forests as a natural seismic metamaterial: Rayleigh wave bandgaps induced by local resonances. Sci. Rep. **6**(December 2015), 1–7 (2016)
9. Comi, C., Driemeier, L.: Metamaterials for crashworthiness of small cars. In: L. Ascione, V. Berardi, L. Feo, F. Fraternali, A. Tralli (eds.) AIMETA 2017 - Proc. 23rd Conf. Ital. Assoc. Theor. Appl. Mech. (2017)
10. Comi, C., Driemeier, L.: Wave propagation in cellular locally resonant metamaterials. Lat. Am. J. Solids Struct. **15**(4), 1–15 (2018)
11. Craster, R.V., Kaplunov, J., Pichugin, A.V.: High-frequency homogenization for periodic media. Proc. R. Soc. A Math. Phys. Eng. Sci. **466**(2120), 2341–2362 (2010)
12. D'Alessandro, L., Belloni, E., D'Alò, G., Daniel, L., Ardito, R., Corigliano, A., Braghin, F.: Modelling and experimental verification of a single phase three-dimensional lightweight locally resonant elastic metamaterial with complete low frequency bandgap. In: 11th Int. Congr. Eng. Mater. Platforms Nov. Wave Phenomena, Metamaterials 2017, pp. 70–77 (2017)
13. Dautray, R., Lions, J.L.: Analyse Mathématique et Calcul Numérique pour les Sciences et les Techniques, vol. 5 : Spectre des Opérateurs. Masson (1988)
14. Hsu, J.C., Wu, T.T.: Lamb waves in binary locally resonant phononic plates with two-dimensional lattices. Appl. Phys. Lett. **90**(20) (2007)
15. Krushynska, A.O., Kouznetsova, V.G., Geers, M.G.D.: Towards optimal design of locally resonant acoustic metamaterials. J. Mech. Phys. Solids **71**(1), 179–196 (2014)
16. Liu, Z., Liu, Z., Zhang, X., Mao, Y., Zhu, Y.Y.: Locally Resonant Sonic Materials. Science (80-.). **289**(September), 1734–1736 (2000)
17. Lv, H., Tian, X., Wang, M.Y., Li, D.: Vibration energy harvesting using a phononic crystal with point defect states. Appl. Phys. Lett. **102**(3), 2013–2016 (2013)

18. Marigo, J.J., Maurel, A., Pham, K., Sbitti, A.: Effective Dynamic Properties of a Row of Elastic Inclusions: The Case of Scalar Shear Waves. J. Elasticity **128**(2), 265–289 (2017)
19. Pham, K., Maurel, A., Marigo, J.J.: Two scale homogenization of a row of locally resonant inclusions - the case of anti-plane shear waves. J. Mech. Phys. Solids **106**, 80–94 (2017)
20. Phani, A.S., Woodhouse, J., Fleck, N.A.: Wave propagation in two-dimensional periodic lattices. J. Acoust. Soc. Am. **119**(4), 1995–2005 (2006)
21. Sanchez-Palencia, E., Sanchez-Hubert, J.: Introduction aux méthodes asymptotiques et à l'homogénéisation. Application à la mécanique des milieux continus. Masson (1992)
22. Wang, G., Wen, X., Wen, J., Shao, L., Liu, Y.: Two-dimensional locally resonant phononic crystals with binary structures. Phys. Rev. Lett. **93**(15) (2004)
23. Xu, X., Barnhart, M.V., Li, X., Chen, Y., Huang, G.: Tailoring visbration suppression bands with hierarchical metamaterials. J. Sound Vib. **442**, 237–248 (2019)